Mechanical impact on the head has an antihypertensive effect

Authors:

Shuhei Murase[1,2,14], Naoyoshi Sakitani[1,14], Takahiro Maekawa[1], Daisuke Yoshino[3], Ayumu Konno[4], Hirokazu Hirai[4], Taku Saito[2], Sakae Tanaka[2], Keisuke Shinohara[5], Takuya Kishi[6], Yuki Yoshikawa[7], Takamasa Sakai[7], Makoto Ayaori[8], Hirohiko Inanami[9], Koji Tomiyasu[10], Toru Ogata[1,11], Atsushi Takashima[12], Masahiro Shinohara[1], Motoshi Nagao[1] and Yasuhiro Sawada[1,13]*

Affiliations:

[1]Department of Rehabilitation for Motor Functions, National Rehabilitation Center for Persons with Disabilities, Tokorozawa, Japan. [2]Department of Orthopaedic Surgery, Graduate School of Medicine, The University of Tokyo, Tokyo, Japan. [3]Division of Advanced Applied Physics, Institute of Engineering, Tokyo University of Agriculture and Technology, Koganei, Japan. [4]Department of Neurophysiology & Neural Repair, Gunma University Graduate School of Medicine, Maebashi, Japan. [5]Department of Cardiovascular Medicine, Kyushu University Graduate School of Medical Sciences, Fukuoka, Japan. [6]Department of Cardiology, Graduate School of Medicine, International University of Health and Welfare, Okawa, Japan. [7]Department of Bioengineering, Graduate School of Engineering, The University of Tokyo, Tokyo, Japan.

20 [8]Tokorozawa Heart Center, Tokorozawa, Japan. [9]Inanami Spine & Joint Hospital/Iwai Orthopaedic
21 Medical Hospital, Iwai Medical Foundation, Tokyo, Japan. [10]Department of Internal Medicine,
22 [11]Center of Sports Science and Health Promotion, [12]Department of Assistive Technology,
23 [13]Department of Clinical Research, National Rehabilitation Center for Persons with Disabilities,
24 Tokorozawa, Japan.
25 [14]These authors contributed equally: Shuhei Murase, Naoyoshi Sakitani.
26 *Correspondence to Yasuhiro Sawada, Department of Clinical Research, National Rehabilitation
27 Center for Persons with Disabilities, 4-1 Namiki, Tokorozawa, Saitama 359-8555, Japan, Tel: +81-
28 4-2995-3100, Fax: +81-4-2995-0355, Email: ys454-ind@umin.ac.jp
29

30 **Abstract**

31 **Nervous cell functions are known to be physiologically regulated by mechanical factors in the**
32 **brain. However, it remains unclear whether mechanical interventions can modulate the**
33 **pathophysiological processes underlying brain-related disorders and modify their**
34 **consequences. Here we show that passive head motion of hypertensive rats, which reproduces**
35 **mechanical accelerations generated at their heads during treadmill running at a moderate**
36 **velocity, decreases the expression of angiotensin II type 1 receptor (AT1R) in astrocytes in**
37 **their rostral ventrolateral medulla (RVLM). This decrease results in lowering their blood**

pressure. Passive head motion generates interstitial fluid movement that is estimated to exert shear stress with average magnitude of a few Pa on cells in rats' brainstem. Fluid shear stress of a relevant magnitude decreases AT1R expression in cultured astrocytes, but not in neuronal cells. Furthermore, in hypertensive rats, inhibition of movement of interstitial fluid by its gelation with reactive polyethylene glycol injected into the RVLM eliminates the ability of passive head motion to decrease their blood pressure and AT1R expression in RVLM astrocytes. Consistent with these results from animal experiments, vertically oscillating chair riding of hypertensive adult humans, which reproduces mechanical accelerations generated at their heads during light jogging or fast walking, lowers their blood pressure. Our findings indicate that moderate mechanical impact on the head has an antihypertensive effect by modulating the function of RVLM astrocytes through interstitial fluid shear stress. We anticipate mechanical regulation to underlie a variety of positive effects of physical exercise on human health, particularly those related to brain functions.

Introduction

Hypertension, which is a major cause of stroke and cardiovascular diseases, is the biggest risk factor for death worldwide[1]. Whereas numerous antihypertensive drugs have been developed and used clinically, physical exercise is known to be effective for the treatment and prevention of essential hypertension[2,3], which comprises the majority (>90%) of human hypertension[4]. Although

57 long-term regulation of blood pressure (BP) has been recognized to be largely dependent on sodium
58 excretion adjusting systems, which mainly involve kidney functions[5], elevated activity of the
59 sympathetic nervous system also importantly contributes to the development of hypertension[6-8].
60 Rostral ventrolateral medulla (RVLM), which is located in the brainstem, plays a critical role in
61 determining the basal activity of the sympathetic nervous system, and its functional integrity is
62 essential for the maintenance of basal vasomotor tone and regulation of BP[6,9]. Angiotensin II (Ang
63 II) is the major bioactive peptide of the renin-angiotensin system (RAS), and is known to regulate
64 BP as well as other biological processes such as cell growth/apoptosis/migration, inflammation, and
65 fibrosis[10]. The biological effects of Ang II are mediated by its interaction with two distinct high-
66 affinity G protein-coupled receptors, Ang II type 1 receptor (AT1R) and type 2 receptor. Of these
67 receptors, AT1R is responsible for most of the known physiological and pathophysiological
68 processes related to Ang II. Whereas RAS is involved in the functional regulation of various
69 "peripheral" organs and tissues such as kidney and vessels, it also regulates brain functions within
70 the blood-brain barrier, including the control and maintenance of sympathetic nerve activity and
71 cognitive ability[11]. In particular, the role of AT1R signaling in the RVLM in cardiovascular
72 regulation has been extensively studied and demonstrated. For example, the pressor/depressor
73 responses to Ang II and Ang II antagonists, injected into the RVLM have been reported to be
74 enhanced in spontaneously hypertensive rats (SHRs)[12,13]. We have previously demonstrated that

75 treadmill running at moderate velocities alleviates the sympathetic nerve activity, involving
76 attenuation of AT1R signaling in the RVLM of stroke-prone spontaneously hypertensive rats
77 (SHRSPs)[14], a substrain of SHRs that exhibit severer hypertension as compared with SHRs[15].
78 However, the details about the changes in AT1R signaling in the RVLM of these hypertensive rats
79 have yet to be elucidated. It remains unclear what type(s) of cells (e.g., neurons or astrocytes) are
80 primarily responsible for the altered AT1R signaling in the RVLM of SHRs or SHRSPs.
81 Furthermore, the causal relationship between the increased AT1R signal activity in the RVLM and
82 high BP in SHRs or SHRSPs in their steady state (i.e., apart from their responses to
83 pharmacological interventions) is left unrevealed.
84 AT1R has also been shown to play a vital role in regulating a variety of physiological or
85 pathological processes, including cellular responses to mechanical perturbations[16,17]. For example,
86 mechanical stretching of cardiac myocytes activates AT1R signaling[18], and fluid shear stress (FSS)
87 of average 1.5 Pa lowers AT1R expression in human vein endothelial cells[19]. Although intervening
88 the Ang II-AT1R system through pharmacological approaches, such as administration of
89 angiotensin-converting enzyme inhibitor or selective AT1R blocker, has been established as an
90 effective therapeutic strategy for hypertension[20], mechano-responsive attenuation of AT1R signaling
91 has not been clinically utilized as an antihypertensive measure.
92 Many of physical workouts, particularly aerobic exercises, involve vertical body motions,

93 which generate mechanical impacts (accelerations) on the head at the time of foot contact with the
94 ground (i.e., landing). The importance of mechanical loads is well established in the physiological
95 regulation of bones, the stiffest organ that only allows tiny deformation[21]. Osteocytes, the
96 mechanosensory cells embedded in bones[22], are assumed to undergo minimal deformations under
97 physiological conditions. We have reported that FSS on osteocytes derived from interstitial fluid
98 flow induced upon physical activity plays an important role in maintaining bone homeostasis[23].
99 Given that the brain is not a rigid organ, minimally deforming forces or stress distribution changes
100 in the brain during exercise or even activity of daily living (e.g., walking) may produce beneficial
101 effects. We have previously shown that in the prefrontal cortex (PFC) of rodents, moderate
102 mechanical impact-induced FSS modulates serotonin signaling in the neurons in situ[24]. Based on
103 these previous findings together with the distribution of interstitial fluid throughout the whole brain,
104 we hypothesized that moderate mechanical impact on the head might have antihypertensive effects
105 involving FSS-mediated modulation of AT1R signaling in the RVLM.
106

107 **Results**

108 **Application of cyclical mechanical impact to the head by passive motion lowers the BP in**
109 **SHRSPs.** To determine the effects of a mechanical intervention of a moderate intensity on BP, we
110 first sought to develop an experimental system that reproduces the impact exerted on the head

111 during rats' treadmill running at a modest velocity (20 m/minute), a typical experimental
112 intervention to test the effects of physical exercise on rats[25,26]. In a recent study, we observed that
113 treadmill running of rats (20 m/minute) generated 5-mm vertical oscillation of their heads with ~1.0
114 x *g* peak accelerations and 2-Hz frequency; therefore, we developed a "passive head motion"
115 (PHM) system to produce 2-Hz 5-mm vertical oscillation exerting 1.0 x *g* acceleration peaks at the
116 heads of rats[24]. In the current study, we examined the effects of mechanical impact on BP in
117 SHRSPs, using the PHM system. Similar to the antihypertensive effect of treadmill running on
118 SHRs or SHRSPs that we and others reported previously[14,25,27], application of PHM (30
119 minutes/day, 28 consecutive days; see Fig. 1a) significantly lowered their BP (Fig. 1b,c) as
120 compared to their controls, whereas HR was not significantly affected by PHM (Fig. 1d).
121 Anesthesia alone (daily 30 minutes) did not significantly alter the BP in SHRSPs (Extended Data
122 Fig. 1a), indicating that the antihypertensive effect resulted specifically from PHM. The anti-cardiac
123 hypertrophy effect of PHM on SHRSPs (Fig. 1e) as well as the lack of these PHM effects on control
124 normotensive rats (Wistar-Kyoto: WKY) (Fig. 1b,c,e) were also consistent with previous reports
125 describing treadmill running as an antihypertensive intervention for SHRs[27]. As was observed in our
126 treadmill running experiments[14], PHM decreased 24-hour urinary norepinephrine excretion of
127 SHRSPs (Fig. 1f). This suggests that PHM mitigates the sympathetic hyperactivity[28]. Collectively,
128 these results support our hypothesis that cyclical moderate mechanical impact on the head has an

129 antihypertensive effect.

130

131 **PHM down-regulates AT1R expression in RVLM astrocytes of SHRSPs.** We then looked into

132 the mechanism of how PHM alleviated the development of hypertension in SHRSPs. We previously

133 reported that down-regulation of AT1R signaling in the RVLM is responsible for the treadmill

134 running-induced sympathoinhibition in SHRSPs[14]. Given the mechanical regulation of AT1R

135 expression in endothelial cells[19], we examined whether PHM modulated AT1R expression in RVLM

136 neurons and astrocytes of SHRSPs. In our histochemical analysis, we defined neuronal nuclei

137 (NeuN)-positive cells as neurons[29] and glial fibrillary acidic protein (GFAP)-positive cells as

138 astrocytes[30]. PHM (30 minutes/day, 28 days) did not significantly change the relative population of

139 AT1R-expressing neurons and astrocytes in the RVLM of WKY rats (Fig. 1g). In contrast, 4-week

140 PHM significantly decreased the expression of AT1R in the astrocytes, but not in the neurons, of

141 SHRSPs' RVLM (Fig. 1h). Notably, AT1R expression in the RVLM neurons was comparable

142 between WKY rats and SHRSPs, either with and without PHM (Fig. 1i). In contrast, AT1R

143 expression was significantly higher in the RVLM astrocytes of SHRSPs without PHM (Fig. 1j,

144 column 3). PHM lowered the AT1R expression in the RVLM astrocytes of SHRSPs to the level

145 equivalent to that of WKY rats (Fig. 1j, columns 1, 2, and 4). Taken together, AT1R expression in

146 RVLM astrocytes appeared to be correlated with the antihypertensive effect of PHM on SHRSPs. In

147 line with this observation, 4-week treadmill running of SHRSPs also decreased the AT1R

148 expression in their RVLM astrocytes, but not neurons (Extended Data Fig. 1b−d).

149

150 **PHM alleviates the sensitivity of RVLM in SHRSPs to Ang II or Ang II antagonist.** We next

151 sought to examine whether the PHM-induced decrease in AT1R expression in the RVLM astrocytes

152 of SHRSPs (Fig. 1j, columns 3 and 4) was functionally relevant to the suppression of AT1R

153 signaling. To this end, we analyzed the pressor responses to Ang II injected into unilateral RVLM of

154 WKY rats and SHRSPs, either subjected to 4-week PHM or left sedentary under anesthesia (30

155 minutes/day, 28 days) (Fig. 2a). As we previously reported[14], SHRSPs without PHM exhibited

156 significantly greater pressor response to Ang II administered to RVLM than WKY rats (Fig. 2b,

157 compare between top and bottom of left panels; Fig. 2c, compare columns 1 and 3). Four-week

158 PHM ameliorated the pressor response to Ang II injected into the RVLM of SHRSPs, but not of

159 WKY rats (Fig. 2b, compare left and right; Fig. 2c, compare columns 1 vs. 2 and 3 vs. 4).

160 Furthermore, depressor responses to Ang II antagonist injected into unilateral RVLM[13] of WHY rats

161 and SHRSPs with and without 4-week PHM appeared to be approximate mirror images of the

162 pressor responses (Fig. 2d,e). These results support the functional relevance of the PHM-induced

163 decrease in AT1R expression in the RVLM astrocytes of SHRSPs (Fig. 1j).

164 To examine whether the increased AT1R expression in the RVLM astrocytes of SHRSPs was

165 associated with their development of hypertension, we manipulated AT1R signaling by introducing
166 exogenous expression of AT1R-associated protein (AGTRAP), which interacts with AT1R and
167 tempers Ang II-mediated signals by promoting AT1R internalization[31]. To this end, we used an
168 adeno-associated virus (AAV)-mediated gene delivery system[32]. AAV serotype 9 (AAV9) vectors
169 were injected locally to transduce RVLM cells (Fig. 3a and Extended Data Fig. 2a). To achieve
170 astrocyte- and neuron-specific gene expression, we used AAV9 vectors that harbored mouse GFAP
171 promoter (AAV-GFAP) and rat neuron-specific enolase (NSE) promoter (AAV-NSE), respectively
172 (Fig. 3a). Because these vectors contained a region encoding GFP and 2A sequence of porcine
173 teschovirus-1 (P2A; self-cleaving peptides[33]) (Fig. 3a), observation of green fluorescence allowed
174 us to identify the cells in which transgene was expressed (Fig. 3b,c and Extended Data Fig. 2a–e).
175 AAV-mediated expression of AGTRAP in astrocytes (Fig. 3b) but not in neurons (Fig. 3c) of
176 bilateral RVLMs in SHRSPs significantly lowered the BP as compared with their control SHRSPs
177 in which only GFP was virally expressed in RVLM astrocytes or neurons (Fig. 3d,e). Furthermore,
178 AAV-mediated expression of AGTRAP in astrocytes, but not neurons, of SHRSPs' bilateral RVLMs
179 decreased 24-hour urinary norepinephrine excretion (Fig. 3f). Injection of control AAV vector
180 (GFAP-control or NSE-control) did not significantly affect the BP of SHRSPs (Extended Data Fig.
181 2f). These results support the importance of AT1R signal intensity in RVLM astrocytes for SHRSPs'
182 development of hypertension and sympathetic hyperactivity, as well as the physiological relevance

183 of PHM-induced decrease in AT1R expression we observed in the RVLM astrocytes of SHRSPs

184 (Fig. 1j).

185

186 **PHM generates low-amplitude pressure waves and induces interstitial fluid movement in rat**

187 **RVLM.** We then sought to determine the physical effects that PHM produced in rat RVLM. To do

188 so, we analyzed local pressure changes using a telemetry pressure sensor (Fig. 4a) as we described

189 previously[24]. PHM generated pressure waves (changes) with ~1.2 mm Hg peak amplitude (Fig.

190 4b−d). Hydrostatic pressure of this magnitude (~1.6 cm H_2O) is unlikely to initiate mechano-

191 responsive signaling in cells[34]. Postulating an analogy to osteocytes embedded in bones, the

192 function of which is known to be modulated by interstitial fluid flow-derived shear stress[23], we have

193 demonstrated that minimal stress distribution changes generate interstitial fluid flow in the brain,

194 resulting in shear stress-mediated regulation of nervous cell functions[24].

195 To analyze the PHM-induced interstitial fluid movement in the RVLM, we injected an iodine-

196 based contrast agent (Isovist®) into the RVLM of anesthetized rats, and tracked its distribution with

197 sequential computed tomography (CT) (Fig. 4e) as we previously did to quantify the movement of

198 intramuscular interstitial fluid[35]. We found that PHM significantly promoted Isovist spreading in the

199 rostral-caudal and dorsal-ventral (*y*- and *z*-axes, Fig. 4f) directions (Fig. 4g,h). In contrast, PHM did

200 not significantly affect the left-right spreading (*x*-axis, Fig. 4f) of Isovist (Fig. 4g,h). As we

201 observed in rat PFC[24], PHM induced interstitial fluid movement in the brainstem in defined
202 directions, rather than in an isotropic manner. Our simulative calculation suggests that PHM
203 subjected RVLM cells to interstitial fluid flow-derived shear stress with an average magnitude of
204 0.59−2.64 Pa (Supplementary Table 1). FSS of this magnitude is known to modify the physiological
205 function of astrocytes[36], leading us to hypothesize that FSS derived from interstitial fluid movement
206 (Fig. 4e−h) mediated the PHM-induced decrease in AT1R expression in RVLM astrocytes (Fig. 1j).
207
208 **FSS on astrocytes decreases AT1R expression in vitro.** To test this hypothesis, we conducted in
209 vitro FSS experiments. Based on our simulation (Supplementary Table 1), we applied pulsatile FSS
210 with an average magnitude of 0.7 Pa to cultured primary astrocytes, which were prepared from
211 astrocyte-GFP mice[37] (Extended Data Fig. 3a), using a system we previously reported[23,24,35,38].
212 Quantitative polymerase chain reaction (qPCR) and immunostaining analyses revealed that FSS
213 application (0.5 Hz, 30 minutes) significantly decreased AT1R expression in astrocytes for at least
214 24 hours (Fig. 5a−c). In contrast, FSS application to Neuro2A cells, which exhibit neuronal
215 phenotypes and morphology[39,40], did not decrease AT1R expression (Extended Data Fig. 3b−d).
216 Consistent with the decreasing effect of FSS on AT1R expression, the binding of fluorescently
217 labeled Ang II to cultured astrocytes was significantly decreased by pre-exposure to 30-minute FSS
218 (Fig. 5d,e). The duration (>24 hours) of FSS effects on AT1R expression in astrocytes (Fig. 5) poses

219 a possibility of cumulative effects of FSS applied repeatedly at 24-hour intervals. Therefore, these
220 in vitro observations suggest that FSS-mediated persistent reduction of AT1R expression is involved
221 in the effects of daily PHM application on BP (Fig. 1b,c) and AT1R expression in the RVLM
222 astrocytes (Fig. 1j) in SHRSPs.
223
224 **Hindrance of interstitial fluid movement by hydrogel introduction in RVLM eliminates the**
225 **ability of PHM to decrease the AT1R expression in RVLM astrocytes and the BP in SHRSPs.**
226 To examine whether interstitial fluid movement in the RVLM mediated the effects of PHM on BP
227 and AT1R expression in RVLM astrocytes of SHRSPs, we modulated local interstitial fluid
228 dynamics. Following the procedure we used to hinder the interstitial fluid movement in mouse
229 PFC[24], we gelled interstitial fluid in situ and deprived its fluidity by microinjecting mutually
230 reactive polyethylene glycol (PEG) gel-precursor (pre-gel) solutions to RVLM (Fig. 6a). Injected
231 pre-gel solution spread over rat RVLM, and gelled the interstitial fluid in situ (Extended Data Fig.
232 4a).
233 Hydrogel introduction in bilateral RVLMs eliminated the ability of PHM to decrease BP (Fig.
234 6b, black and orange lines; Fig. 6c, columns 2 and 3), urinary norepinephrine excretion (Fig. 6d,
235 columns 2 and 3), and AT1R expression in the RVLM astrocytes (Fig. 6e, bottom 2 rows; Fig. 6f,
236 columns 2 and 3) in SHRSPs. In contrast, hydrogel introduction increased BP (Fig. 6b, blue and

237 orange lines; Fig. 6c, columns 1 and 3), norepinephrine excretion (Fig. 6d, columns 1 and 3), and
238 AT1R expression in the RVLM astrocytes (Fig. 6e, top 2 rows; Fig. 6f, columns 1 and 3) of
239 SHRSPs subjected to PHM. AT1R expression in the RVLM neurons of SHRSPs remained unaltered
240 irrespective of the combination of PHM and hydrogel introduction (Fig. 6e,g). These results suggest
241 that hydrogel introduction in the RVLM disrupts the mechanism mediating the PHM-induced
242 decrease in BP, norepinephrine excretion, and AT1R expression in the RVLM astrocytes of
243 SHRSPs.

244 We previously showed that gelation only inhibits the fluidity of the fluid but does not restrict
245 the diffusion of small molecules inside the gel[24,41]. Consistently, hydrogel introduction did not
246 apparently delay or attenuate the depressor response to Ang II antagonist injected to the RVLM
247 (Extended Data Fig. 4b−d), indicating rapid solute diffusivity through the hydrogels. As was the
248 case with mouse PFC[24], gelation by injecting PEG solution did not affect overall cell number or
249 apoptosis in RVLM (Extended Data Fig. 4e,f), and survival or apoptosis of RVLM astrocytes
250 (Extended Data Fig. 4g,h) and neurons (Extended Data Fig. 4i,j). Collectively, the loss of PHM
251 effects by hydrogel introduction in bilateral RVLMs of SHRSPs (Fig. 6b−f) is likely to result from
252 hydrogel-mediated alteration in interstitial fluid dynamics, rather than decreased cell viability
253 caused by impaired nutrient supply or removal of metabolic wastes.
254

255 **Vertically oscillating chair riding (VOCR) lowers BP in hypertensive adult humans.** The
256 results from our animal experiments reveal the antihypertensive effect of mechanical accelerations
257 generated at the head during treadmill running at a moderate velocity. This prompted us to test
258 whether mechanical impact on the head lowered BP in hypertensive humans. As we observed light
259 jogging or fast walking (locomotion at the velocity of 7 km/hour) typically produce ~2 Hz vertical
260 acceleration waves with an amplitude of ~1.0 x *g* at the person's head (Extended Data Fig. 5a, top),
261 we constructed a chair that could vertically oscillate at the frequency of 2 Hz (Extended Data Fig.
262 5b) and produce ~1.0 x *g* acceleration waves at the head of the occupant (Extended Data Fig. 5a,
263 bottom).

264 Given that previous reports regarding antihypertensive effects of aerobic exercise typically
265 recommend ≥3−4 days per week (frequency) and ≥30 minutes per session or day (duration)[3], we set
266 our regimen of VOCR as 3 days/week (Monday, Wednesday, and Friday unless needed to assign
267 otherwise for particular reasons such as public holidays) and 30 minutes/day. Our study of protocol
268 1, in which we simply compared the subjects' BP and HR before and after 4-week (12 times)
269 VOCR (Extended Data Fig. 5c), showed that VOCR decreased BP in hypertensive humans (Fig.
270 7a).

271 We then conducted a human study of protocol 2, in which we followed the changes in subjects'
272 BP and HR more minutely (Extended Data Fig. 5d). Encouraged by the positive results from the

273 study of protocol 1, we adopted the same VOCR regimen as to its frequency (3 days/week) and
274 duration (30 minutes/day). Participants were subjected to serial blood sampling to measure plasma
275 catecholamines (epinephrine, norepinephrine, and dopamine) and renin activity, and serum
276 aldosterone and C-reactive protein (CRP) before and after the intervention period (Extended Data
277 Fig. 5d). To conduct the 2nd blood sampling on the next day of the last bout of VOCR, the
278 intervention period was extended from 4 weeks (total 12 times, typically 26 days) to 4.5 weeks
279 (total 14 times, 30−31 days) because blood sampling could not be done during weekends at our
280 hospital. BP, both systolic and diastolic, and MAP immediately after the intervention period
281 significantly decreased as compared with those immediately before the intervention period (Fig.
282 7b). Furthermore, we also observed an antihypertensive effect of VOCR when we defined "BP of
283 the week" to reliably detect the trends by reducing the influences from interday BP variability (see
284 Methods) (Fig. 7c and Extended Data Fig. 6a). Notably, the post-intervention follow-up showed that
285 the BP-lowering effect apparently persisted for 4 weeks, but not 5 weeks, after the last bout of
286 VOCR (Fig. 7c). Similar to our animal study, we did not observe significant changes in HR by the
287 VOCR intervention (Fig. 7a−c). Significant differences were not detected in the blood levels of
288 catecholamines, aldosterone, renin activity, and CRP between before and after the VOCR
289 intervention (Extended Data Fig. 6b).

290 Collectively, our studies of protocols 1 and 2 suggest that VOCR, which reproduces

291 mechanical impact exerted on the head during light jogging or fast walking, has an antihypertensive
292 effect in hypertensive humans. Importantly, in none of 21 subjects (Supplementary Table 2),
293 apparent adverse events, including motion sickness and low back pain, were observed or manifested
294 in relation to the VOCR intervention.
295

296 **Discussion**

297 Essential hypertension is defined as high BP in which secondary causes including renovascular
298 disease, renal failure, pheochromocytoma, and primary aldosteronism are not present. It accounts
299 for >90% of human cases of hypertension, resulting from combinations of multiple genetic and
300 environmental factors[4]. Recently, brain (dys)function has been implicated in the pathogenesis of
301 essential hypertension; however, the details of their molecular link remain unclear[42]. Physical
302 exercise is proven to be effective as a therapeutic/preventative measure for essential hypertension[3].
303 Although the antihypertensive effect of physical exercise has been shown to involve normalization
304 of sympathetic hyperactivity in the brain[43], it is still unclear whether exercise directly modulates
305 brain function. In this study, PHM, which reproduced mechanical accelerations generated at the
306 head during treadmill running, allowed us to dissect bodily activity-derived physical effects.
307 Whereas AT1R signaling in both neurons and astrocytes of the RVLM have been reported to be
308 involved in regulating BP[44,45], we observed that AT1R expression in RVLM astrocytes was

309 increased in SHRSPs as compared to that in WKY rats (Fig. 1j). In contrast, AT1R expression in
310 RVLM neurons was comparable between WKY rats and SHRSPs (Fig. 1i), although AT1R
311 expression in RVLM neurons has been shown to play an important role in other animal model(s) of
312 hypertension[44]. Together with the decreases in BP and urinary epinephrine excretion of SHRSPs in
313 which RVLM astrocytes were transduced with AGTRAP gene (Fig. 3d−f), the intensity of AT1R
314 signaling in RVLM astrocytes appears to be critically involved in the pathogenesis of hypertension
315 and sympathetic hyperactivity in SHRSPs.

316 Four-week PHM decreased urinary norepinephrine excretion and AT1R expression in RVLM
317 astrocytes of SHRSPs to the levels almost equivalent to those of WKY rats (Fig. 1f,j). However,
318 PHM only partially alleviated the development of hypertension in SHRSPs to the extent similar to
319 the antihypertensive effects of treadmill running we and others previously reported[14,25] (Fig. 1b,c).
320 Therefore, it is evident that factors other than AT1R signaling in RVLM astrocytes contribute to the
321 pathogenesis of essential hypertension.

322 AT1R expression in cultured astrocytes decreased upon FSS application (Fig. 5a−c). This was
323 consistent with our findings that PHM and treadmill running decreased in AT1R expression in
324 RLVM astrocytes of SHRSPs (Fig. 1j and Extended Data Fig. 1d). However, the AT1R expression
325 level in RVLM astrocytes was low in WKY rats even without PHM (Fig. 1j), and this may raise a
326 concern regarding the physiological relevance of our in vitro FSS experiments using cultured

327 astrocytes. Yet, it has been reported that cultured astrocytes typically exhibit increased "reactivity",
328 and do not fully recapitulate physiological astrocytes in vivo[46]. We suggest that the FSS-induced
329 decrease in AT1R expression in cultured astrocytes we observed represents physiological functions
330 of astrocytes, despite that their increased basal AT1R expression may relate to unphysiological
331 aspects of two-dimensional culture on stiff substrates (culture plastics). Cells in static culture are
332 exposed to a complete absence of FSS, which may not be physiologically realized in vivo. Previous
333 reports describe increased extracellular fluid in brains of hypertensive humans[47] and altered
334 dynamics of intracerebral interstitial fluid of SHRs[48]. Aberrant regulation of RVLM astrocytes'
335 function that relates to altered interstitial fluid movement-derived FSS may underlie the
336 pathogenesis of essential hypertension.

337 PHM did not significantly alter the AT1R expression in SHRSPs' RVLM neurons (Fig. 1i), and
338 FSS did not decrease AT1R expression in cultured Neuro2A cells (Extended Data Fig. 3b−d). Yet,
339 we do not suspect that these results represent the absence of sensitivity of neurons to FSS or other
340 type(s) of mechanical stimulation, particularly because we observed PHM- and FSS-induced
341 internalization of 5-HT_{2A} receptor expressed in mouse PFC neurons and Neuro2A cells,
342 respectively[24]. Alternatively, we speculate that PHM and FSS may mitigate hyperexpression of
343 AT1R related to aforementioned pathological status of SHRSPs' RVLM astrocytes or
344 unphysiological nature of cultured astrocytes. In line with this notion, PHM did not significantly

345 affect the AT1R expression in RVLM astrocytes in normotensive WKY rats (Fig. 1j). Relevantly,
346 we and others have reported mechanical loading (in vivo)- or FSS (in vitro)- induced alleviation of
347 inflammatory processes[23,49], which can transcriptionally increase AT1R expression[50].

348 Whereas the amplitude of pressure waves that PHM generated in rat RVLM was tiny (Fig.
349 4b−d), the magnitude of interstitial fluid movement-derived shear stress in rat RVLM appeared
350 comparable with that of FSS previously reported for vascular endothelium[51,52], interstitium of
351 bone[21] and skeletal muscle[35] (Supplementary Table 1b). Consistent with the lack of strict cell
352 specificity in many of cellular responses to mechanical forces[53], FSS-induced decrease in AT1R
353 expression, which was reported in vascular cells[19], was also observed in cultured astrocytes. Taken
354 together, we speculate that there may be common homeostasis-regulatory mechanisms at the
355 cellular level that involve fluid flow-derived shear stress of ~0.5 to a few Pa.

356 Based on our hypothesis concerning the similarity in the pathogenesis of high BP between
357 human essential hypertension and SHRSPs, we conducted human studies in which we intended to
358 reproduce the mechanical impact on the head that lowered the BP in SHRSPs. Although the
359 mechanism behind the apparent antihypertensive effect of VOCR remains to be determined, the
360 significant role of interstitial fluid dynamics in the RVLM, which we demonstrated by our animal
361 experiments, might be shared between humans and rats or other animals (Extended Data Fig. 7).
362 Whereas plasma catecholamine levels were not significantly changed by the VOCR intervention

363 (Extended Data Fig. 6b), it is possible that urinary epinephrine measures collected over 24 hours in
364 our rat PHM experiments (Fig. 1f, 3f, and 6d) enhanced our ability to capture the sympathetic nerve
365 activity under ‘‘everyday-life’’ ambulatory conditions[54].

366 As the phrase “Exercise is Medicine” indicates, physical exercise is broadly useful to maintain
367 human health. Many of aerobic exercises, including walking and running, involve impact-
368 generating bodily actions creating sharp accelerations at the head upon foot contacting with the
369 ground. Therefore, their beneficial effects as therapeutic/preventative procedures for a variety of
370 brain function-related diseases and health disorders may rely at least partly on modest changes in
371 mechanical stress distribution in the brain, which may prompt optimal FSS on intracerebral nervous
372 cells. While we have recently demonstrated that brain function can be physiologically regulated by
373 mechanical forces[24], alterations in interstitial fluid movement-derived shear stress may underlie the
374 pathogenesis of various brain disorders, particularly those related to physical inactivity or aging.

375 **Limitation of study.** There are several limitations of this study. We were unable to test the response
376 of primary neurons, which were prepared from mouse cerebral cortex or hippocampus, to FSS of
377 relevant magnitudes (0.59−2.64 Pa, see Supplementary Table 1b) because of their easy detachment
378 from the substrates by FSS. As an alternative of cultured neuronal cells, we tested Neuro2A cells,
379 which stably adhered to the substrates through FSS of magnitudes up to ~1 Pa[24].

380 We did not comprehensively analyze the effects of PHM on brain functions, but focused on the

381 study of RVLM. PHM may modulate AT1R signaling in other brain regions that participate in the
382 regulation of sympathetic nerve activity, including the anteroventral third ventricle, paraventricular
383 nucleus of the hypothalamus, and nucleus tractus solitarii[6,9]. Nonetheless, elimination of PHM
384 effects on BP and urinary norepinephrine excretion by hydrogel introduction in RVLM (Fig. 6b−d)
385 supports the critical role for RVLM. Because hydrogel may exert yet unknown effects, experiments
386 of hydrogel introduction may not entirely prove the contribution of interstitial fluid movement. For
387 example, hydrogel introduction may alter the stiffness and elasticity of extracellular matrix, which
388 are known to affect the neurological physiology, pathology, and development[55]. Although further
389 studies are required to address these issues, our findings suggest that mechanical factors can be a
390 therapeutic target within the blood-brain barrier, the accessibility to which of antihypertensive drugs
391 appears variable and controversial[56].

392 Unlike the case of PHM in rats, VOCR of humans generates vertical accelerations at various
393 body parts in addition to the head. Therefore, we cannot preclude the possibility that the
394 antihypertensive effect of VOCR is mediated by mechanical regulation of tissues and organs other
395 than the brain. Furthermore, our clinical studies of protocol 1 and 2 are based on a small number of
396 subjects (Supplementary Table 2) with a fixed condition (frequency of 2 Hz, peak acceleration of
397 ~1.0 x *g*, 30 minutes/day, 3 days/week, 12−14 rides), and need further analysis with a much larger
398 sample size and varying conditions to determine optimal VOCR. Still, application of vertical

mechanical impacts with moderate magnitudes is expected to be highly safe with minimal possibility of adverse effects, providing a novel therapeutic/preventative strategy for physical disorders including those that are resistant to conventional treatments such as drug administration. Notably, our approach utilizing mechanical interventions may bring considerable benefits to those who cannot receive benefits from exercise because of physical disabilities.

Data availability

All data are included in this article and its supplementary information files. Raw data are available from the corresponding author upon reasonable request.

Acknowledgements

We thank K. Nakanishi, K. Hamamoto, and N. Kume for their consistent support. This work was in part supported by Intramural Research Fund from the Japanese Ministry of Health, Labour and Welfare; Grants-in-Aid for Scientific Research from the Japan Society for the Promotion of Science (15H01820, 15H04966, and 18H04088 to Y.S; 17H02127 and 18H03138 to T.O.; 19K06899 to A.K.); MEXT-Supported Program for the Strategic Research Foundation at Private Universities, 2015−2019 from the Japanese Ministry of Education, Culture, Sports, Science and Technology (S1511017 to Y.S. and T.O.); Brain Mapping by Integrated Neurotechnologies for Disease Studies

from the Japan Agency for Medical Research and Development (AMED Brain/MINDS, JP20dm0207057 to H.H.).

Author contributions

S.M. and N.S. conducted most of the experiments. Y.S. conceived the research, designed the study, and led the project with help from M.N. and M.S. T.K. provided technical advice for all the experiments involving measurement of cardiovascular parameters. S.M., N.S., T.K., M.S. and Y.S. wrote the manuscript. T.M. and A.T. contributed to the design and construction of the machine for PHM. D.Y. helped in vitro FSS experiments and carried out simulative calculation of in vivo FSS. T.S. and Y.Y. developed and provided the PEG hydrogel system. A.K. and H.H. prepared and provided AAV vectors. K.T., T.K., M.A., H.I., and T.O. contributed to the human studies. K.S., T.S., S.T. M.S., T.O., and M.N. provided technical, advisory and financial support.

Competing interests

The authors declare no competing interest. S.M., T.M., T.O., A.T., and Y.S. joined the application of a patent for the vertically oscillating chair, which has been awarded in Japan (JP6592834) and filed internationally (US16/616,935; EP18806753.2; CN201880033284.0; IN201927048891).

References

1. Lim, S.S., *et al.* A comparative risk assessment of burden of disease and injury attributable to 67 risk factors and risk factor clusters in 21 regions, 1990-2010: a systematic analysis for the Global Burden of Disease Study 2010. *Lancet* **380**, 2224-2260 (2012).
2. Hagberg, J.M., Park, J.J. & Brown, M.D. The role of exercise training in the treatment of hypertension: an update. *Sports Med* **30**, 193-206 (2000).
3. Pescatello, L.S., MacDonald, H.V., Lamberti, L. & Johnson, B.T. Exercise for hypertension: a prescription update integrating existing recommendations with emerging research. *Curr Hypertens Rep* **17**, 87 (2015).
4. Carretero, O.A. & Oparil, S. Essential hypertension. Part I: definition and etiology. *Circulation* **101**, 329-335 (2000).
5. Guyton, A.C. Abnormal renal function and autoregulation in essential hypertension. *Hypertension* **18**, III49-53 (1991).
6. Guyenet, P.G. The sympathetic control of blood pressure. *Nat Rev Neurosci* **7**, 335-346 (2006).
7. Grassi, G., Mark, A. & Esler, M. The sympathetic nervous system alterations in human hypertension. *Circ Res* **116**, 976-990 (2015).
8. Malpas, S.C. Sympathetic nervous system overactivity and its role in the development of cardiovascular disease. *Physiol Rev* **90**, 513-557 (2010).
9. Dampney, R.A. Functional organization of central pathways regulating the cardiovascular system. *Physiol Rev* **74**, 323-364 (1994).
10. Fyhrquist, F. & Saijonmaa, O. Renin-angiotensin system revisited. *J Intern Med* **264**, 224-236 (2008).
11. Forrester, S.J., *et al.* Angiotensin II signal transduction: an update on mechanisms of physiology and pathophysiology. *Physiol Rev* **98**, 1627-1738 (2018).
12. Ito, S., Komatsu, K., Tsukamoto, K., Kanmatsuse, K. & Sved, A.F. Ventrolateral medulla AT1 receptors support blood pressure in hypertensive rats. *Hypertension* **40**, 552-559 (2002).
13. Muratani, H., Ferrario, C.M. & Averill, D.B. Ventrolateral medulla in spontaneously hypertensive rats: role of angiotensin II. *Am J Physiol* **264**, R388-395 (1993).
14. Kishi, T., *et al.* Exercise training causes sympathoinhibition through antioxidant effect in the rostral ventrolateral medulla of hypertensive rats. *Clin Exp Hypertens* **34**, 278-283 (2012).
15. Nabika, T., Ohara, H., Kato, N. & Isomura, M. The stroke-prone spontaneously hypertensive rat: still a useful model for post-GWAS genetic studies? *Hypertens Res* **35**, 477-484 (2012).
16. Lu, X., *et al.* Effects of local mechanical stimulation on coronary artery endothelial function and angiotensin II type 1 receptor in pressure or flow-overload. *J Hypertens* **31**, 720-729 (2013).

470 17. Galie, P.A., Russell, M.W., Westfall, M.V. & Stegemann, J.P. Interstitial fluid flow and cyclic
471 strain differentially regulate cardiac fibroblast activation via AT1R and TGF-β1. *Exp Cell Res*
472 **318**, 75-84 (2012).
473 18. Zou, Y.*, et al.* Mechanical stress activates angiotensin II type 1 receptor without the
474 involvement of angiotensin II. *Nat Cell Biol* **6**, 499-506 (2004).
475 19. Ramkhelawon, B.*, et al.* Shear stress regulates angiotensin type 1 receptor expression in
476 endothelial cells. *Circ Res* **105**, 869-875 (2009).
477 20. Li, E.C., Heran, B.S. & Wright, J.M. Angiotensin converting enzyme (ACE) inhibitors versus
478 angiotensin receptor blockers for primary hypertension. *Cochrane Database Syst Rev*,
479 CD009096 (2014).
480 21. Weinbaum, S., Cowin, S.C. & Zeng, Y. A model for the excitation of osteocytes by mechanical
481 loading-induced bone fluid shear stresses. *J Biomech* **27**, 339-360 (1994).
482 22. Tatsumi, S.*, et al.* Targeted ablation of osteocytes induces osteoporosis with defective
483 mechanotransduction. *Cell Metab* **5**, 464-475 (2007).
484 23. Miyazaki, T.*, et al.* Mechanical regulation of bone homeostasis through p130Cas-mediated
485 alleviation of NF-κB activity. *Sci Adv* **5**, eaau7802 (2019).
486 24. Ryu, Y.*, et al.* Mechanical regulation underlies effects of exercise on serotonin-induced
487 signaling in the prefrontal cortex neurons. *iScience* **23**, 100874 (2020).
488 25. Minami, N.*, et al.* Effects of exercise and β-blocker on blood pressure and baroreflexes in
489 spontaneously hypertensive rats. *Am J Hypertens* **16**, 966-972 (2003).
490 26. Kim, S.E.*, et al.* Treadmill exercise prevents aging-induced failure of memory through an
491 increase in neurogenesis and suppression of apoptosis in rat hippocampus. *Exp Gerontol* **45**,
492 357-365 (2010).
493 27. Bertagnolli, M.*, et al.* Exercise training reduces sympathetic modulation on cardiovascular
494 system and cardiac oxidative stress in spontaneously hypertensive rats. *Am J Hypertens* **21**,
495 1188-1193 (2008).
496 28. Chidsey, C.A., Braunwald, E. & Morrow, A.G. Catecholamine excretion and cardiacstores of
497 norepinephrine in congestive heart failure. *Am J Med* **39**, 442-451 (1965).
498 29. Mullen, R.J., Buck, C.R. & Smith, A.M. NeuN, a neuronal specific nuclear protein in
499 vertebrates. *Development* **116**, 201-211 (1992).
500 30. Freeman, M.R. Specification and morphogenesis of astrocytes. *Science* **330**, 774-778 (2010).
501 31. Tamura, K.*, et al.* The physiology and pathophysiology of a novel angiotensin receptor-binding
502 protein ATRAP/Agtrap. *Curr Pharm Des* **19**, 3043-3048 (2013).
503 32. Huda, F.*, et al.* Distinct transduction profiles in the CNS via three injection routes of AAV9 and
504 the application to generation of a neurodegenerative mouse model. *Mol Ther Methods Clin Dev*
505 **1**, 14032 (2014).

506 33. Tang, X., *et al.* "Self-cleaving" 2A peptide from porcine teschovirus-1 mediates cleavage of
507 dual fluorescent proteins in transgenic Eimeria tenella. *Vet Res* **47**, 68 (2016).
508 34. Tworkoski, E., Glucksberg, M.R. & Johnson, M. The effect of the rate of hydrostatic pressure
509 depressurization on cells in culture. *PLoS One* **13**, e0189890 (2018).
510 35. Saitou, K., *et al.* Local cyclical compression modulates macrophage function in situ and
511 alleviates immobilization-induced muscle atrophy. *Clin Sci (Lond)* **132**, 2147-2161 (2018).
512 36. Maneshi, M.M., *et al.* Mechanical stress activates NMDA receptors in the absence of agonists.
513 *Sci Rep* **7**, 39610 (2017).
514 37. Gong, S., *et al.* A gene expression atlas of the central nervous system based on bacterial
515 artificial chromosomes. *Nature* **425**, 917-925 (2003).
516 38. Yoshino, D., Sakamoto, N., Takahashi, K., Inoue, E. & Sato, M. Development of Novel Flow
517 Chamber to Study Endothelial Cell Morphology: Effects of shear flow with uniform spatial
518 gradient ondistribution of focal adhesion. *J Biomech Sci Eng* **8**, 233-243 (2013).
519 39. Goshima, Y., Ohsako, S. & Yamauchi, T. Overexpression of Ca^{2+}/calmodulin-dependent protein
520 kinase II in Neuro2A and NG108-15 neuroblastoma cell lines promotes neurite outgrowth and
521 growth cone motility. *J Neurosci* **13**, 559-567 (1993).
522 40. Yun, J., *et al.* Neuronal Per Arnt Sim (PAS) domain protein 4 (NPAS4) regulates neurite
523 outgrowth and phosphorylation of synapsin I. *J Biol Chem* **288**, 2655-2664 (2013).
524 41. Fujiyabu, T., Toni, F., Li, X., Chung, U.I. & Sakai, T. Three cooperative diffusion coefficients
525 describing dynamics of polymer gels. *Chem Commun (Camb)* **54**, 6784-6787 (2018).
526 42. Jennings, J.R., Muldoon, M.F. & Sved, A.F. Is the brain an early or late component of essential
527 hypertension? *Am J Hypertens* (2020).
528 43. Joyner, M.J. & Green, D.J. Exercise protects the cardiovascular system: effects beyond
529 traditional risk factors. *J Physiol* **587**, 5551-5558 (2009).
530 44. Jancovski, N., *et al.* Angiotensin type 1A receptor expression in C1 neurons of the rostral
531 ventrolateral medulla contributes to the development of angiotensin-dependent hypertension.
532 *Exp Physiol* **99**, 1597-1610 (2014).
533 45. Guo, F., *et al.* Astroglia are a possible cellular substrate of angiotensin(1-7) effects in the rostral
534 ventrolateral medulla. *Cardiovasc Res* **87**, 578-584 (2010).
535 46. Liddelow, S.A. & Barres, B.A. Reactive astrocytes: production, function, and therapeutic
536 potential. *Immunity* **46**, 957-967 (2017).
537 47. Maclullich, A.M., *et al.* Higher systolic blood pressure is associated with increased water
538 diffusivity in normal-appearing white matter. *Stroke* **40**, 3869-3871 (2009).
539 48. Bedussi, B., *et al.* Enhanced interstitial fluid drainage in the hippocampus of spontaneously
540 hypertensive rats. *Sci Rep* **7**, 744 (2017).
541 49. Hahn, C. & Schwartz, M.A. Mechanotransduction in vascular physiology and atherogenesis.
542 *Nat Rev Mol Cell Biol* **10**, 53-62 (2009).

543 50. Elton, T.S. & Martin, M.M. Angiotensin II type 1 receptor gene regulation: transcriptional and
544 posttranscriptional mechanisms. *Hypertension* **49**, 953-961 (2007).
545 51. Galie, P.A., van Oosten, A., Chen, C.S. & Janmey, P.A. Application of multiple levels of fluid
546 shear stress to endothelial cells plated on polyacrylamide gels. *Lab Chip* **15**, 1205-1212 (2015).
547 52. Kadohama, T., Nishimura, K., Hoshino, Y., Sasajima, T. & Sumpio, B.E. Effects of different
548 types of fluid shear stress on endothelial cell proliferation and survival. *J Cell Physiol* **212**,
549 244-251 (2007).
550 53. Iskratsch, T., Wolfenson, H. & Sheetz, M.P. Appreciating force and shape-the rise of
551 mechanotransduction in cell biology. *Nat Rev Mol Cell Biol* **15**, 825-833 (2014).
552 54. Hughes, J.W., Watkins, L., Blumenthal, J.A., Kuhn, C. & Sherwood, A. Depression and anxiety
553 symptoms are related to increased 24-hour urinary norepinephrine excretion among healthy
554 middle-aged women. *J Psychosom Res* **57**, 353-358 (2004).
555 55. Li, S.C.*, et al.* Tissue elasticity bridges cancer stem cells to the tumor microenvironment
556 through microRNAs: implications for a "watch-and-wait" approach to cancer. *Curr Stem Cell*
557 *Res Ther* **12**, 455-470 (2017).
558 56. Kishi, T., Hirooka, Y. & Sunagawa, K. Sympathoinhibition caused by orally administered
559 telmisartan through inhibition of the AT(1) receptor in the rostral ventrolateral medulla of
560 hypertensive rats. *Hypertens Res* **35**, 940-946 (2012).
561 57. Huang, N. & Bonn, D. Viscosity of a dense suspension in Couette flow. *J Fluid Mech* **590**, 497-
562 507 (2007).
563 58. Sugiyama, S.*, et al.* Computational simulation of convection-enhanced drug delivery in the
564 non-human primate brainstem: a simple model predicting the drug distribution. *Neurol Res* **35**,
565 773-781 (2013).
566 59. Yao, W., Shen, Z. & Ding, G. Simulation of interstitial fluid flow in ligaments: comparison
567 among Stokes, Brinkman and Darcy models. *Int J Biol Sci* **9**, 1050-1056 (2013).
568 60. Tarbell, J.M. & Shi, Z.-D. Effect of the glycocalyx layer on transmission of interstitial flow
569 shear stress to embedded cells. *Biomech Model Mechanobiol* **12**, 111-121 (2013).
570 61. Sakai, K.*, et al.* Overexpression of eNOS in NTS causes hypotension and bradycardia in vivo.
571 *Hypertension* **36**, 1023-1028 (2000).
572 62. Kishi, T.*, et al.* Overexpression of eNOS in the RVLM causes hypotension and bradycardia via
573 GABA release. *Hypertension* **38**, 896-901 (2001).
574 63. Paxinos, G. & Watson, C. *The rat brain in stereotaxic coordinates* (Academic Press, 1998).
575 64. Hirooka, Y., Polson, J.W. & Dampney, R.A. Pressor and sympathoexcitatory effects of nitric
576 oxide in the rostral ventrolateral medulla. *J Hypertens* **14**, 1317-1324 (1996).
577 65. Shinohara, Y.*, et al.* Effects of neutralizing antibody production on AAV-PHP.B-mediated
578 transduction of the mouse central nervous system. *Mol Neurobiol* **56**, 4203-4214 (2019).

579 66. Shinohara, Y., Ohtani, T., Konno, A. & Hirai, H. Viral vector-based evaluation of regulatory
580 regions in the neuron-specific enolase (NSE) promoter in mouse cerebellum in vivo.
581 *Cerebellum* **16**, 913-922 (2017).
582 67. Konno, A.*, et al.* Mutant ataxin-3 with an abnormally expanded polyglutamine chain disrupts
583 dendritic development and metabotropic glutamate receptor signaling in mouse cerebellar
584 Purkinje cells. *Cerebellum* **13**, 29-41 (2014).
585 68. Matsuzaki, Y.*, et al.* Neurotropic Properties of AAV-PHP.B are shared among diverse inbred
586 strains of mice. *Mol Ther* **27**, 700-704 (2019).
587 69. Sakitani, N.*, et al.* Application of consistent massage-kike perturbations on mouse calves and
588 monitoring the resulting intramuscular pressure changes. *J Vis Exp* e59475 (2019).
589 70. Liu, C., De Luca, A., Rosso, A. & Talon, L. Darcy's law for yield stress fluids. *Phys Rev Lett*
590 **122**, 245502 (2019).
591 71. Schildge, S., Bohrer, C., Beck, K. & Schachtrup, C. Isolation and culture of mouse cortical
592 astrocytes. *J Vis Exp* e50079 (2013).
593 72. Umemura, S.*, et al.* The Japanese Society of Hypertension guidelines for the management of
594 hypertension (JSH 2019). *Hypertens Res* **42**, 1235-1481 (2019).

595

596 **Figures and figure legends**

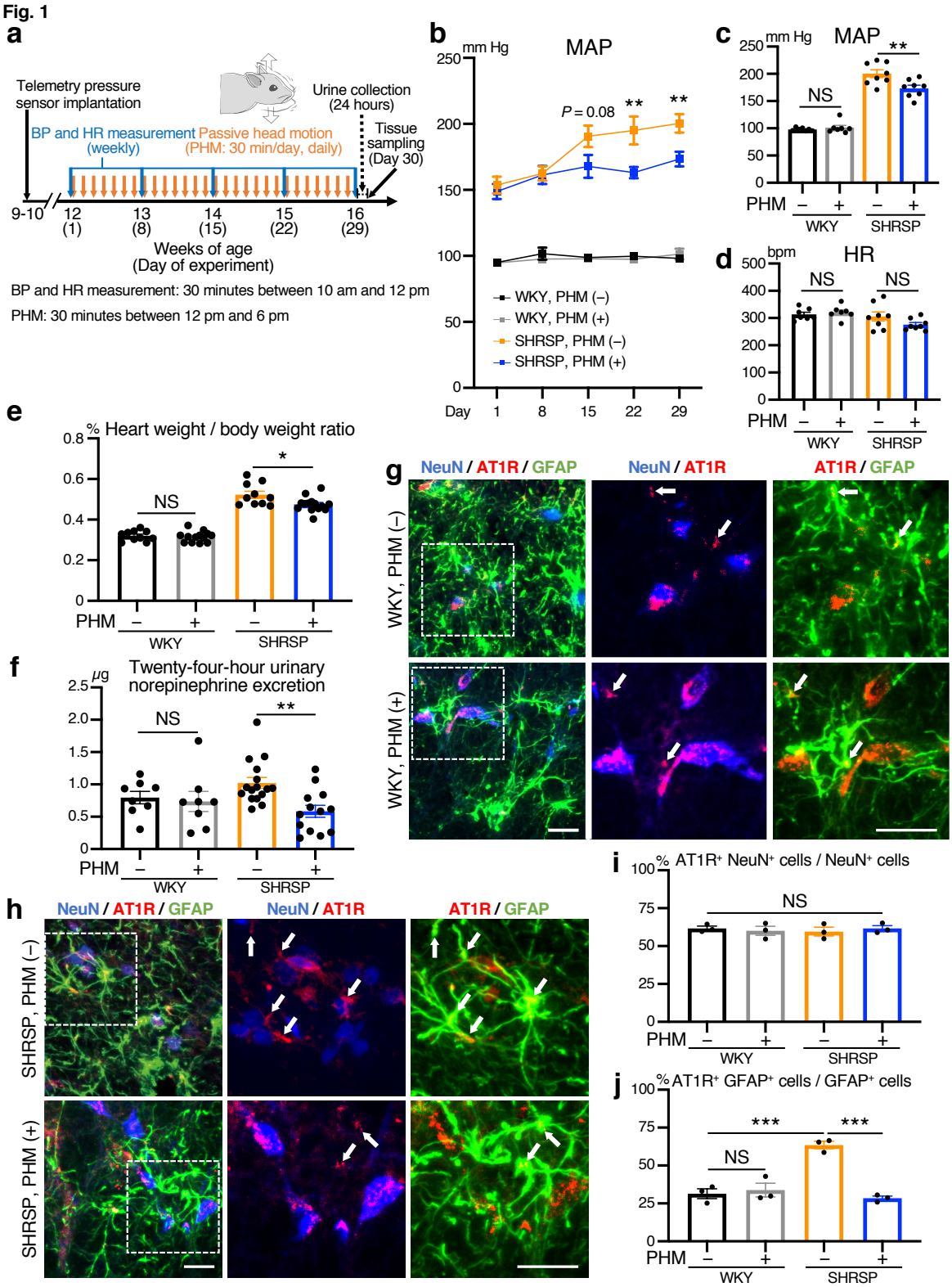

Fig. 1 | Application of cyclical mechanical impact to the head by passive motion lowers the BP

599 **in SHRSPs, and AT1R expression in their RVLM astrocytes. a,** Schematic representation of

600 experimental protocol for analysis of the effects of PHM on BP in rats. **b,c,** Time courses **(b)** and

601 values on Day 29 **(c)** of MAP of WKY rats and SHRSPs, subjected to either daily PHM or

602 anesthesia only (**b**: $P = 0.0814$ for Day15, $P = 0.0052$ for Day 22, and $P = 0.0046$ for Day 29. **c**: P

603 $= 0.9739$ for column 1 vs. 2 and $P = 0.0046$ for column 3 vs. 4. $n = 7$ rats for each group of WKY

604 and $n = 8$ rats for each group of SHRSP). **d,** HR values on Day 29 ($P = 0.9650$ for column 1 vs. 2

605 and $P = 0.2362$ for column 3 vs. 4. $n = 7$ rats for each group of WKY and $n = 8$ rats for each group

606 of SHRSP). **e,** Relative heart weight (heart weight / whole body weight) measured on Day 30 [$P =$

607 0.9866 for column 1 vs. 2 and $P = 0.0152$ for column 3 vs. 4. $n = 10$ rats for WKY, PHM (−); $n = 13$

608 rats for WKY, PHM (+); $n = 10$ rats for SHRSP, PHM (−); $n = 14$ rats for SHRSP, PHM (+)]. **f,**

609 Twenty-four-hour (Day 29 to Day 30) urinary norepinephrine excretion [$P = 0.9854$ for column 1

610 vs. 2 and $P = 0.0085$ for column 3 vs. 4. $n = 8$ rats for each group of WKY; $n = 16$ rats for SHRSP,

611 PHM (−); $n = 13$ rats for SHRSP, PHM (+)]. **g,h,** Micrographic images of anti-NeuN (blue), anti-

612 GFAP (green) and anti-AT1R (red) immunostaining of the RVLM of WKY rats **(g)** and SHRSPs

613 **(h)**, either left sedentary (top) or subjected to PHM (bottom) under anesthesia (30 minutes/day, 28

614 days). Higher magnification images (center and right) refer to the areas indicated by dotted

615 rectangles in low magnification images (left). Arrows point to anti-AT1R immunosignals that

616 overlap with anti-GFAP, but not anti-NeuN, immunosignals in merged images. Scale bars, 50 μm.

617 Images are representative of three rats. **i,j,** Quantification of AT1R-positive neurons **(i)** and

618 astrocytes **(j)** in the RVLM of WKY rats and SHRSPs, either left sedentary or subjected to PHM.

619 Fifty NeuN-positive ($NeuN^+$) cells and one hundred GFAP-positive ($GFAP^+$) cells were analyzed

620 for each rat (**i**: $P = 0.7803$. **j**: $P = 0.9455$ for column 1 vs. 2, $P = 0.0004$ for column 1 vs. 3, and $P =$

621 0.0002 for column 3 vs. 4. $n = 3$ rats for each group). Data are presented as mean ± s.e.m. $^{*}P < 0.05$;

622 $^{**}P < 0.01$; $^{***}P < 0.001$; NS, not significant; one-way ANOVA with Tukey's post hoc multiple

623 comparisons test.

Extended Data Fig. 1

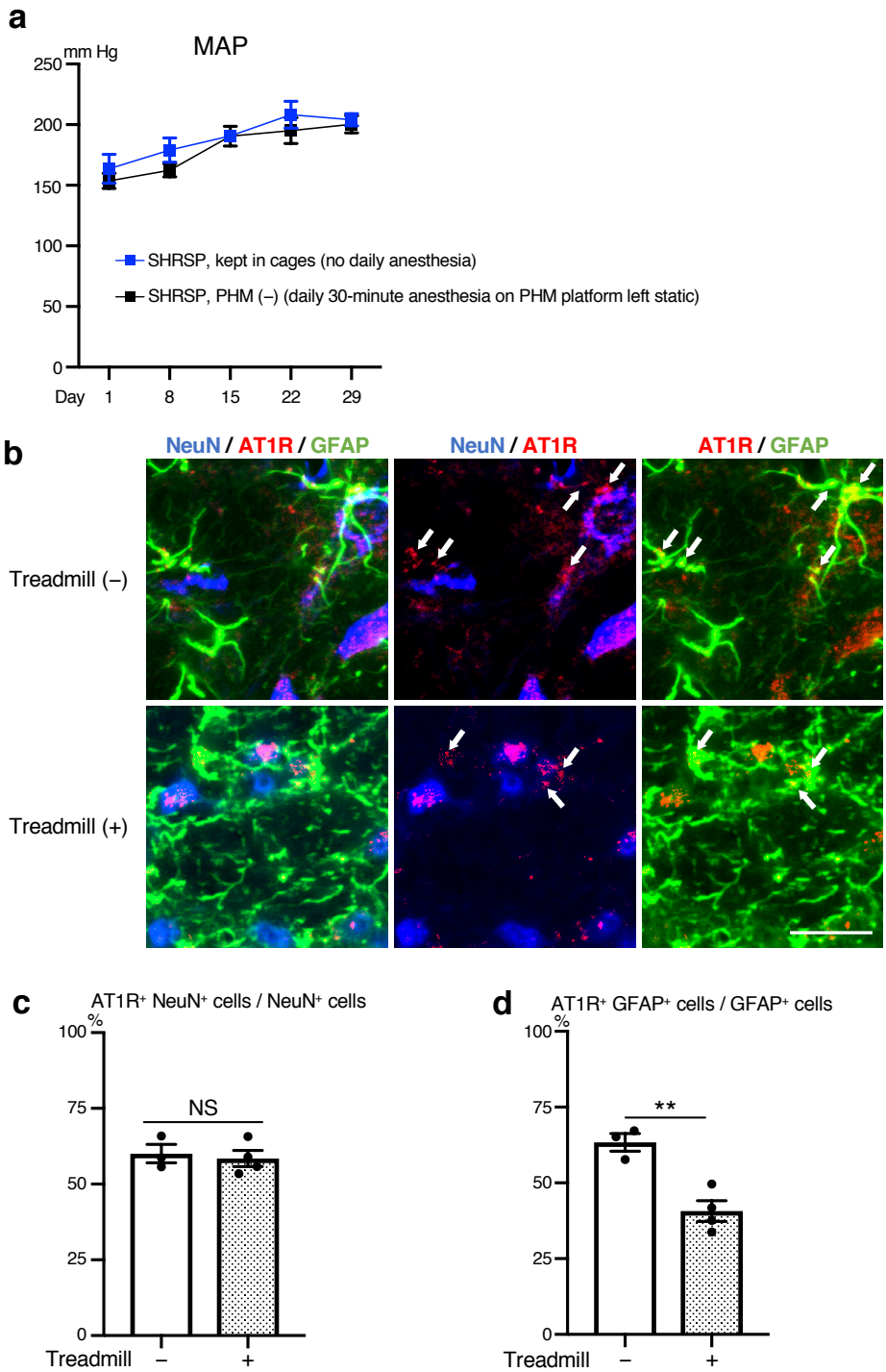

Extended Data Fig. 1 | Daily anesthesia alone does not affect BP, and treadmill running decreases AT1R expression in the RVLM astrocytes in SHRSPs. a, Time courses of MAP of

627 SHRSPs either routinely kept in cages (no anesthesia) or subjected to daily anesthesia on the

628 platform of PHM machine without turning on its switch [PHM (−)] [n = 6 rats for no daily

629 anesthesia and n = 8 rats for PHM (−)]. **b,** Micrographic images anti-NeuN (blue), anti-GFAP

630 (green) and anti-AT1R (red) immunostaining of the RVLM of SHRSPs, either placed in the static

631 treadmill machine or subjected to treadmill running at the velocity of 20 m/minute (30 minutes/day,

632 28 days). Arrows point to anti-AT1R immunosignals that overlap with anti-GFAP, but not anti-

633 NeuN, immunosignals in merged images. Scale bar, 50 μm. Images are representative of three or

634 four rats. **c,d,** Quantification of AT1R-positive neurons **(c)** and astrocytes **(d)** in the RVLM of

635 SHRSPs with or without 4-week treadmill running. Fifty $NeuN^+$ cells and one hundred $GFAP^+$ cells

636 were analyzed for each rat [**c**: P = 0.7056. **d**: P = 0.0048. n = 3 rats for treadmill (−) and n = 4 rats

637 for treadmill (+)]. Data are presented as mean ± s.e.m. **P < 0.01; NS, not significant, unpaired

638 two-tailed Student's t-test.

Fig. 2

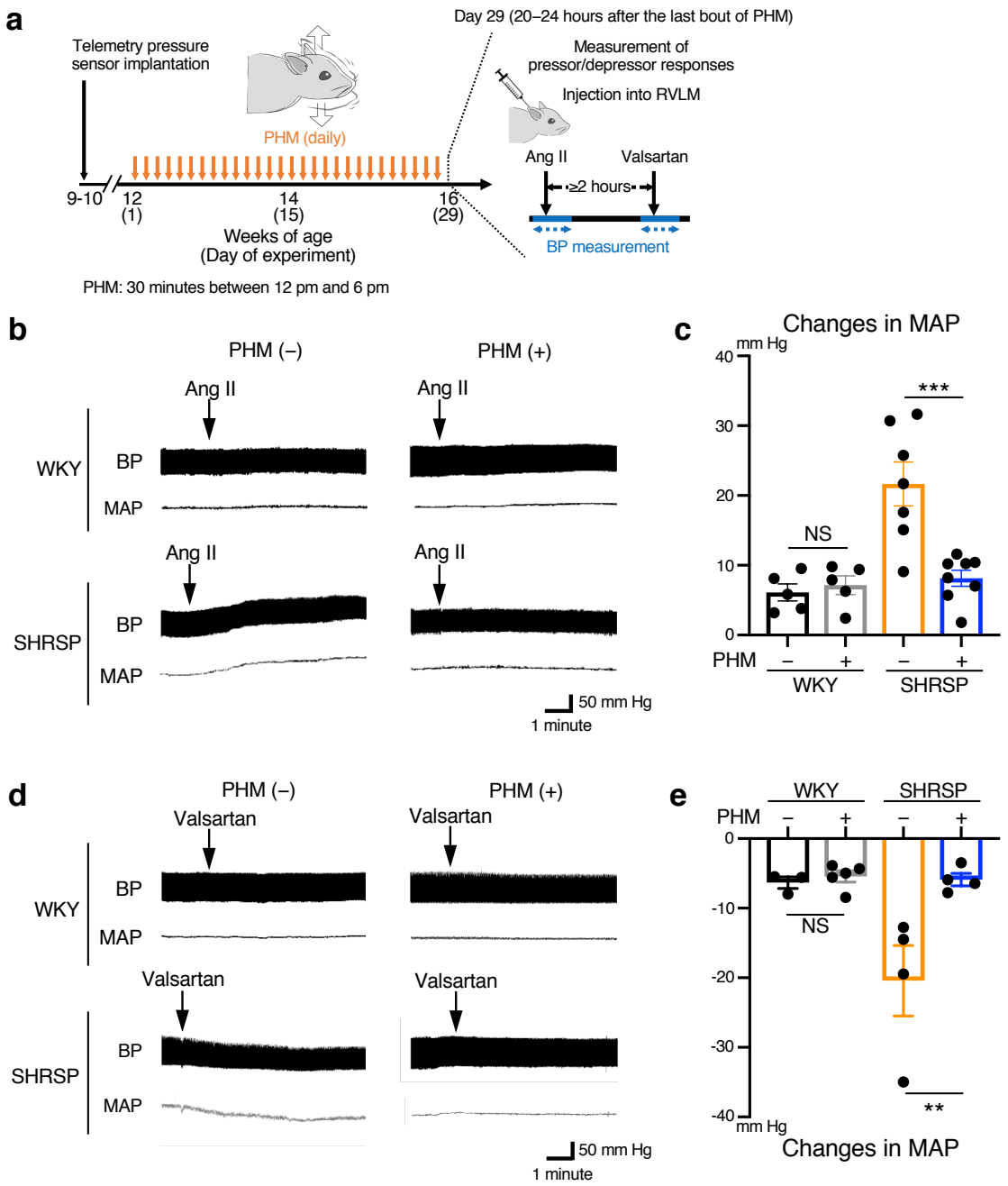

639

640 **Fig. 2 | PHM alleviates the sensitivity of RVLM in SHRSPs to Ang II or valsartan. a,**

641 Schematic representation of experimental protocol for analysis of the effects of PHM on the

642 sensitivity to Ang II or valsartan injected into unilateral RVLM. Ang II (100 pmol) was injected into

643 the unilateral RVLM of WKY rats and SHRSPs, either left sedentary (daily anesthesia) or subjected
644 to PHM (30 minutes/day, 28 days), with their BP monitored under urethane anesthesia. Injection of
645 valsartan (100 pmol) into the RVLM was conducted at least 2 hours after the injection of Ang II. **b,**
646 Representative trajectories of BP (top in each panel) and MAP (bottom in each panel). Arrows point
647 to the time of the initiation of RVLM injection of Ang II. **c,** Quantification of MAP change caused
648 by Ang II injection [$P = 0.9876$ for column 1 vs. 2 and $P = 0.0003$ for column 3 vs. 4. $n = 5$ rats for
649 each group of WKY; $n = 7$ rats for SHRSP, PHM (−); $n = 8$ rats for SHRSP, PHM (+)]. **d,e,** Effects
650 of RVLM injection of valsartan (100 pmol) examined as in **(b,c)** [**e**: $P = 0.9953$ for column 1 vs. 2
651 and $P = 0.0099$ for column 3 vs. 4. $n = 3$ rats for WKY, PHM (−); $n = 5$ rats for WKY, PHM (+); n
652 $= 4$ rats for each group of SHRSP]. Data are presented as mean ± s.e.m. $^{**}P < 0.01$; $^{***}P < 0.001$;
653 NS, not significant; one-way ANOVA with Tukey's post hoc multiple comparisons test.

Fig. 3

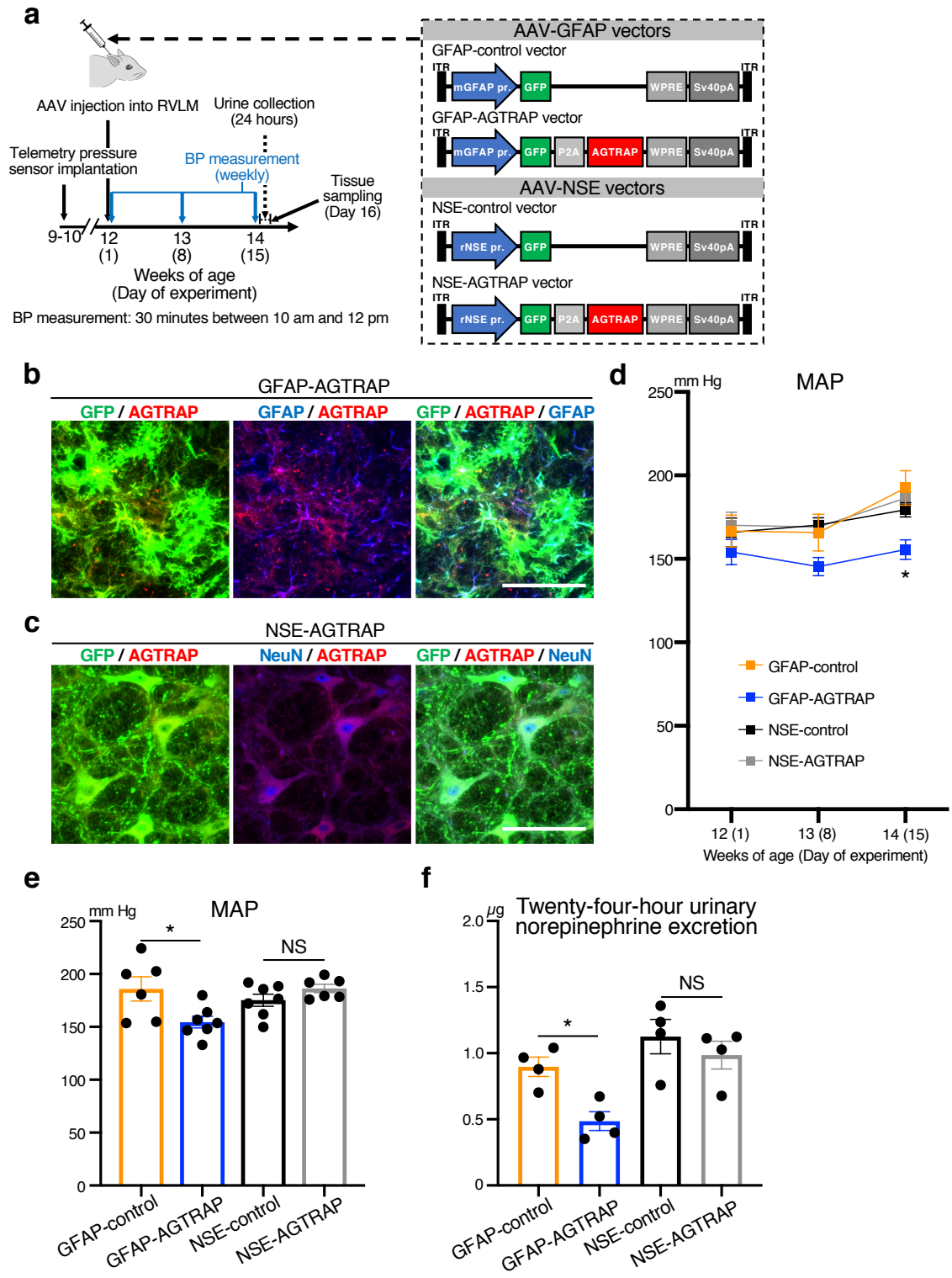

654

655 **Fig. 3 | AAV-mediated expression of AGTRAP in RVLM astrocytes, but not neurons, lowers**

656 **the BP in SHRSPs. a,** Schematic representation of experimental protocol for analysis of the effects
657 of AAV-mediated transduction of RVLM astrocytes or neurons with AGTRAP gene. ITR; inverted
658 terminal repeat. **b,c,** Astrocyte- **(b)** and neuron- **(c)** specific transgene expression by RVLM
659 injection of AAV9 vectors. Micrographic images of GFP (green) and anti-GFAP **(b)** or anti-NeuN
660 **(c)** immunostaining (blue) of RVLM of SHRSPs 15 days after the injection of AAV9 vectors
661 indicated at the top of each panel. Scale bars, 50 μm. Images are representative of three rats. **d–f,**
662 Time courses **(d)** and values on Day 15 **(e)** of MAP (**d**: $P = 0.0229$ for Day 14. **e**: $P = 0.0229$ for
663 column 1 vs. 2 and $P = 0.6864$ for column 3 vs. 4. $n = 6$ rats for GFAP-control; $n = 7$ rats for
664 GFAP-AGTRAP; $n = 7$ rats for NSE-control; $n = 6$ rats for NSE-AGTRAP), and 24-hour urinary
665 norepinephrine excretion **(f)** ($P = 0.0497$ for column 1 vs. 2 and $P = 0.7455$ for column 3 vs. 4. $n =$
666 4 rats for each group) of SHRSPs subjected to RVLM injection of AAV9 vectors. Data are
667 presented as mean ± s.e.m. *$P < 0.05$; NS, not significant, one-way ANOVA with Tukey's post hoc
668 multiple comparisons test.

Extended Data Fig. 2

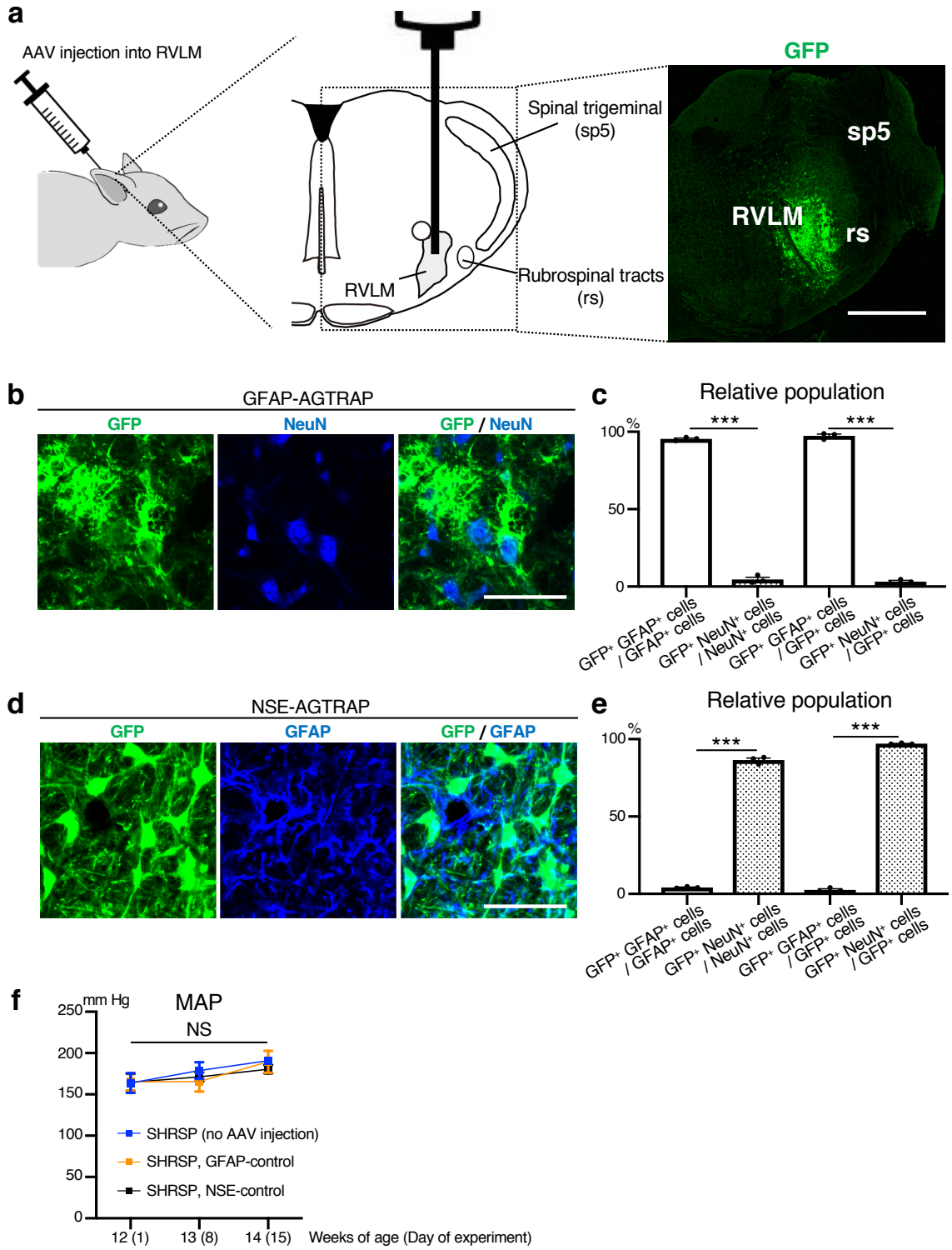

Extended Data Fig. 2 | AAV-mediated transduction of RVLM astrocytes or neurons in

671 **SHRSPs. a,** Schematic representation of injection of AAV9 vectors to RVLM. Micrographic image
672 is representative of three rats analyzed in Fig. 3b (15 days after the RVLM injection of GFAP-
673 AGTRAP vector). GFP-derived fluorescence indicates cells expressing the transgene. Scale bar, 1
674 mm. **b,c,** Efficiency and specificity of astrocyte-specific expression of the transgene. **(b)**
675 Micrographic images of GFP (green) and anti-NeuN immunostaining (blue) of RVLM of SHRSPs
676 analyzed in Fig. 3b. Scale bar, 50 μm. Images are representative of three rats. **(c)** Quantification of
677 the efficiency and specificity of transgene expression. The relative populations (%) of GFP- GFAP-
678 double positive (GFP^+ $GFAP^+$) or GFP- NeuN-double positive (GFP^+ $NeuN^+$) cells were calculated
679 by referring their numbers to those of GFP^+, $GFAP^+$ or $NeuN^+$ cells ($P < 0.0001$ for column 1 vs. 2
680 and $P < 0.0001$ for column 3 vs. 4. $n = 3$ rats for each group). **d,e,** Efficiency and specificity of
681 neuron-specific expression of the transgene. **(d)** Micrographic images of GFP (green) and anti-
682 GFAP immunostaining (blue) of RVLM of SHRSPs analyzed in Fig. 3c. Scale bar, 50 μm. Images
683 are representative of three rats. **(e)** The efficiency and specificity quantified as in **(c)** ($P < 0.0001$for
684 column 1 vs. 2 and $P < 0.0001$ for column 3 vs. 4.). **f,** BP in SHRSPs injected with control vectors.
685 BP was measured and MAP was quantified as in Fig. 1b ($P = 0.9803$ for Week 12, $P = 0.5914$ for
686 Week 13, and $P = 0.4693$ for Week 14. $n = 6$ rats for no AAV injection; $n = 6$ rats for GFAP-control;
687 $n = 7$ rats for NSE-control). The data for blue line are identical with those demonstrated with blue
688 line in Extended Data Fig. 1a. Data are presented as mean ± s.e.m. ***$P < 0.001$; NS, not

689 significant; unpaired two-tailed Student's *t*-test **(c,e)** or one-way ANOVA with Tukey's post hoc

690 multiple comparisons test **(f)**.

Fig. 4

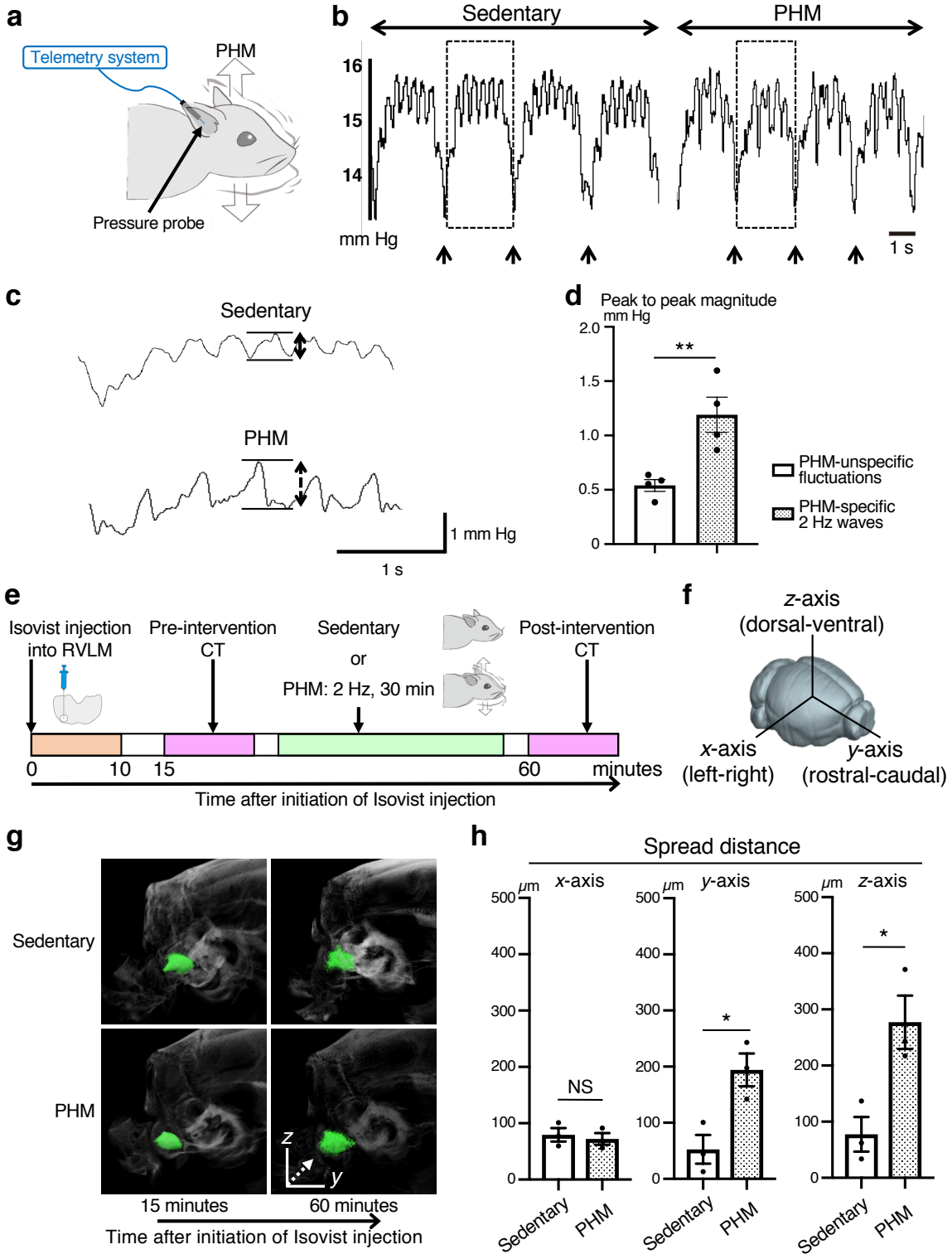

691

692 **Fig. 4 | PHM generates pressure waves of low amplitude, but facilitates interstitial fluid**

movement (flow) in rat RVLM. a, Schematic representation of pressure measurement in rat RVLM. **b,** Representative pressure waves recorded in rat RVLM during sedentary condition and PHM. Arrows point to the time of transition from inhalation to exhalation detected by simultaneous respiration monitoring. Scale bar, 1 s. Images are representative of three independent experiments with similar results. **c,** Respiration-unsynchronized pressure changes. Respiration-synchronized pressure waves indicated by dotted rectangles in **(b)** are presented with high magnification. Right-angled scale bar, 1 s / 1 mm Hg. Note that 2-Hz pressure waves indicated by a two-headed dotted line arrow were specifically generated during PHM. **d,** Magnitude of PHM-specific and -unspecific pressure changes unsynchronized with respiration. Peak to peak magnitudes indicated by two-headed arrows in **(c)** were quantified ($P = 0.0089$. $n = 4$ rats for each group, 10 segments analyzed for each rat). **e,** Schematic representation of experimental protocol for μCT analysis of Isovist injected in rat RVLM. **f,** Definition of *x*-(left-right), *y*-(rostral-caudal), and *z*-(dorsal-ventral) axes used in this study. **g,** Representative Isovist spreading presented on X-ray images. Isovist clusters are indicated by green. Images are representative of three rats. A dotted line arrow indicates the main direction of spreading in this sample. **h,** Quantification of Isovist spreading along each axis (left chart: $P = 0.6666$. middle chart: $P = 0.0218$. right chart: $P = 0.0244$. $n = 3$ rats for each group). Data are presented as mean ± s.e.m. $^{*}P < 0.05$; $^{**}P < 0.01$; NS, not significant, unpaired two-tailed Student's *t*-test.

Supplementary Table 1

a

Property	Value
Pressure changes (ΔP; mmHg)	1.19
Viscosity (μ; mPa•s)	1–20 ♯
Spread distance along x-axis per each PHM cycle (Δx; μm)	–0.002
Spread distance along y-axis per each PHM cycle (Δy; μm)	0.039
Spread distance along z-axis per each PHM cycle (Δz; μm)	0.055
Velocity of interstitial fluid flow along x-axis ($u_{\infty,x}$; μm/s)	–0.004
Velocity of interstitial fluid flow along y-axis ($u_{\infty,y}$; μm/s)	0.079
Velocity of interstitial fluid flow along z-axis ($u_{\infty,z}$; μm/s)	0.111

b

FSS (τ_x) along x-axis at the cell surface:

$$\tau_x = \frac{\mu u_{\infty,x}}{\sqrt{K_{p,x}}}$$

$$K_{p,x} = \frac{\mu u_{\infty,x} \Delta x}{\Delta P}$$

, where $K_{p,x}$ is the Darcy permeability of brain tissue along x-axis.

The shear stresses along y- and z-axes can be calculated in a similar manner.

When the values listed in **a** are introduced in these equations, the magnitude of FSS is estimated as 0.59–2.64 Pa.

Supplementary Table 1 | Simulative calculation of the magnitude of PHM-generated FSS on rat RVLM cells. a, Values referenced for simulative calculation of the magnitude of FSS that PHM generated in rat RVLM. All referenced values except viscosity (marked with ♯) were drawn from

715 analyses with IBP measurement and Isovist-enhanced μCT scanning (Fig. 4d,h). The property of

716 interstitial fluid viscosity was referenced from previous studies[57-59]. **b,** Calculation of the magnitude

717 of FSS generated by PHM. FSS (τ) at the cell surface can be calculated as reported previously[60].

Fig. 5

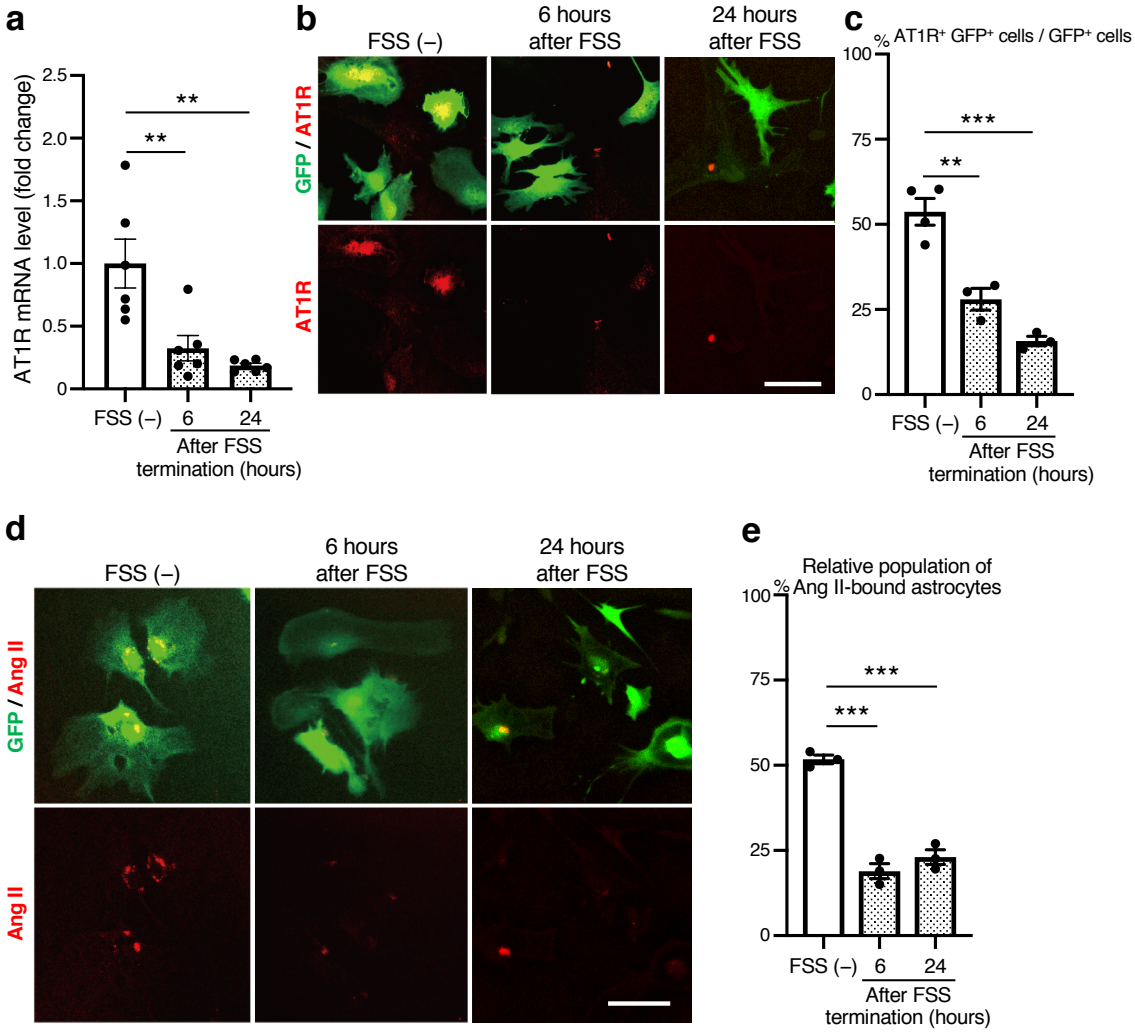

Fig. 5 | FSS on cultured astrocytes decreases their AT1R expression and Ang II-binding potential in vitro. a–c, AT1R expression in cultured astrocytes with or without exposure to FSS. Astrocytes prepared from astrocyte-GFP mice, either left unexposed or exposed to pulsatile FSS (average 0.7 Pa, 0.5 Hz, 30 minutes) were analyzed 6 and 24 hours after the cessation of 30-minute FSS application. **(a)** AT1R mRNA expression levels normalized against GAPDH expression and scaled as the mean value from control samples (cells left unexposed to FSS) set as 1 (P = 0.0050 for

column 1 vs. 2 and $P = 0.0011$ for column 1 vs. 3. $n = 6$). **(b)** Microscopic images of anti-AT1R (red) and anti-GFP (green) immunostaining. Images are representative of three or four independent experiments with similar results. Scale bar, 50 μm. **(c)** Relative population of AT1R- GFP-double positive ($AT1R^+$ GFP^+) cells were quantified as a ratio to total GFP-positive (GFP^+) cells in each sample [$P = 0.0021$ for column 1 vs. 2 and $P = 0.0002$ for column 1 vs. 3. >100 GFP-positive cells were analyzed in each sample; $n = 4$ for FSS (−), $n = 3$ for 6 and 24 hours after FSS]. **d,e,** Effect of FSS on astrocytes' Ang II-binding potential. Cultured astrocytes were either left unexposed or exposed to FSS as in **(a−c)**. Six and twenty-four hours after the cessation of 30-minute FSS application, cells were subjected to fluorescent Ang II binding assay. **(d)** Microscopic images representative of three independent experiments with similar results. Scale bar, 50 μm. **(e)** GFP-positive cells with punctate red fluorescence (TAMRA-Ang II-bound astrocytes) were quantified as a ratio (%) to total GFP-positive cells in each sample ($P < 0.0001$ for column 1 vs. 2 and $P = 0.0001$ for column 1 vs. 3. 100 GFP-positive cells were analyzed in each sample; $n = 3$ for each group). Data are presented as mean ± s.e.m. $^{**}P < 0.01$, $^{***}P < 0.001$, one-way ANOVA with Tukey's post hoc multiple comparisons test.

Extended Data Fig. 3

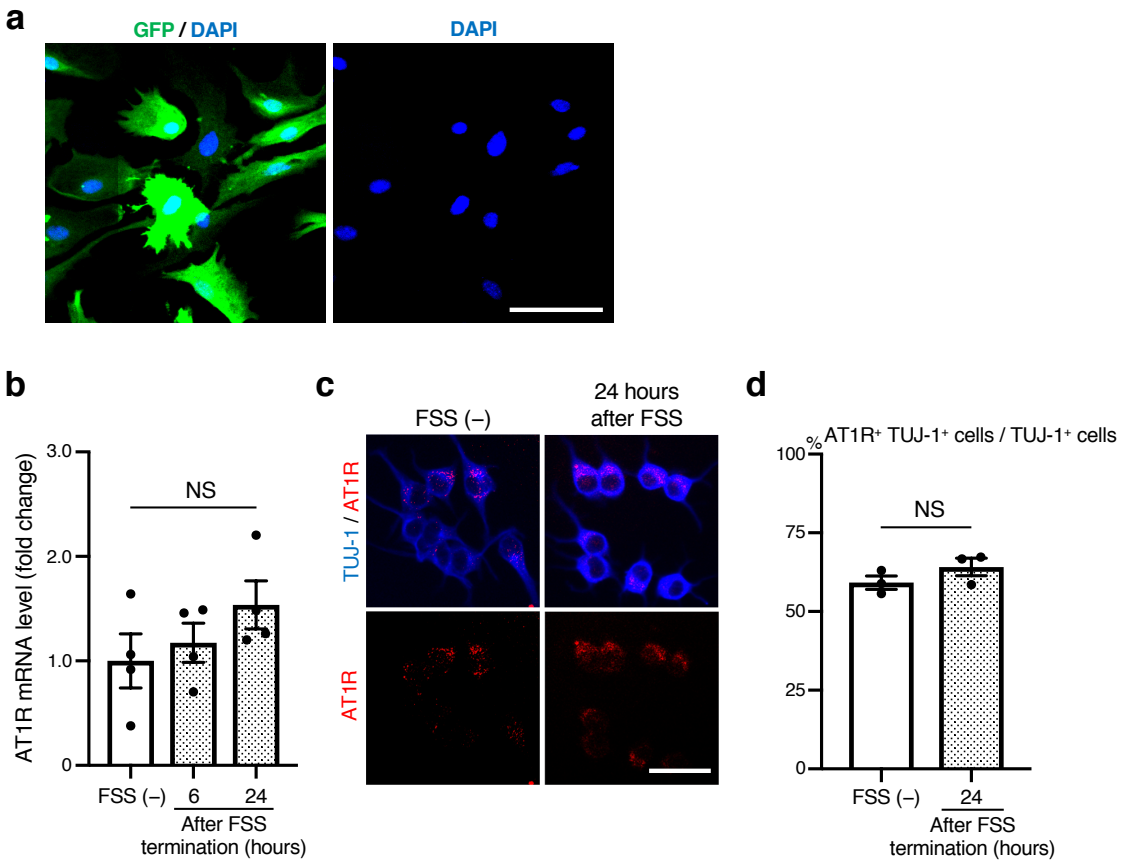

740

741 **Extended Data Fig. 3 | Preparation of astrocyte-enriched primary culture, and lack of**

742 **decreasing effect of FSS on AT1R expression in cultured neuronal cells. a,** Representative

743 micrographic image of anti-GFP immunostaining (green) and DAPI staining (blue) of astrocyte-

744 enriched culture prepared from astrocyte-GFP mice. Scale bar, 50 μm. Note that most of the cells

745 are GFP-positive. **b–d,** Effects of FSS on AT1R expression in Neuro2A cells analyzed as in Fig.

746 5a–c. **(b)** AT1R mRNA expression levels ($P = 0.2834$. $n = 4$). **(c)** Micrographic images

747 representative of three independent experiments with similar results. Scale bar, 50 μm. **(d)** Relative

748 population of AT1R- TUJ-1-double positive ($AT1R^+$ $TUJ\text{-}1^+$) cells quantified as a ratio to total TUJ-

749 1-positive (TUJ-1^{+}) cells in each sample (P = 0.2308. >100 TUJ-1-positive cells were analyzed in

750 each sample; n = 3). Data are presented as mean ± s.e.m. NS, not significant, one-way ANOVA with

751 Tukey's post hoc multiple comparisons test **(b)** or unpaired two-tailed Student's *t*-test **(d)**.

Fig. 6

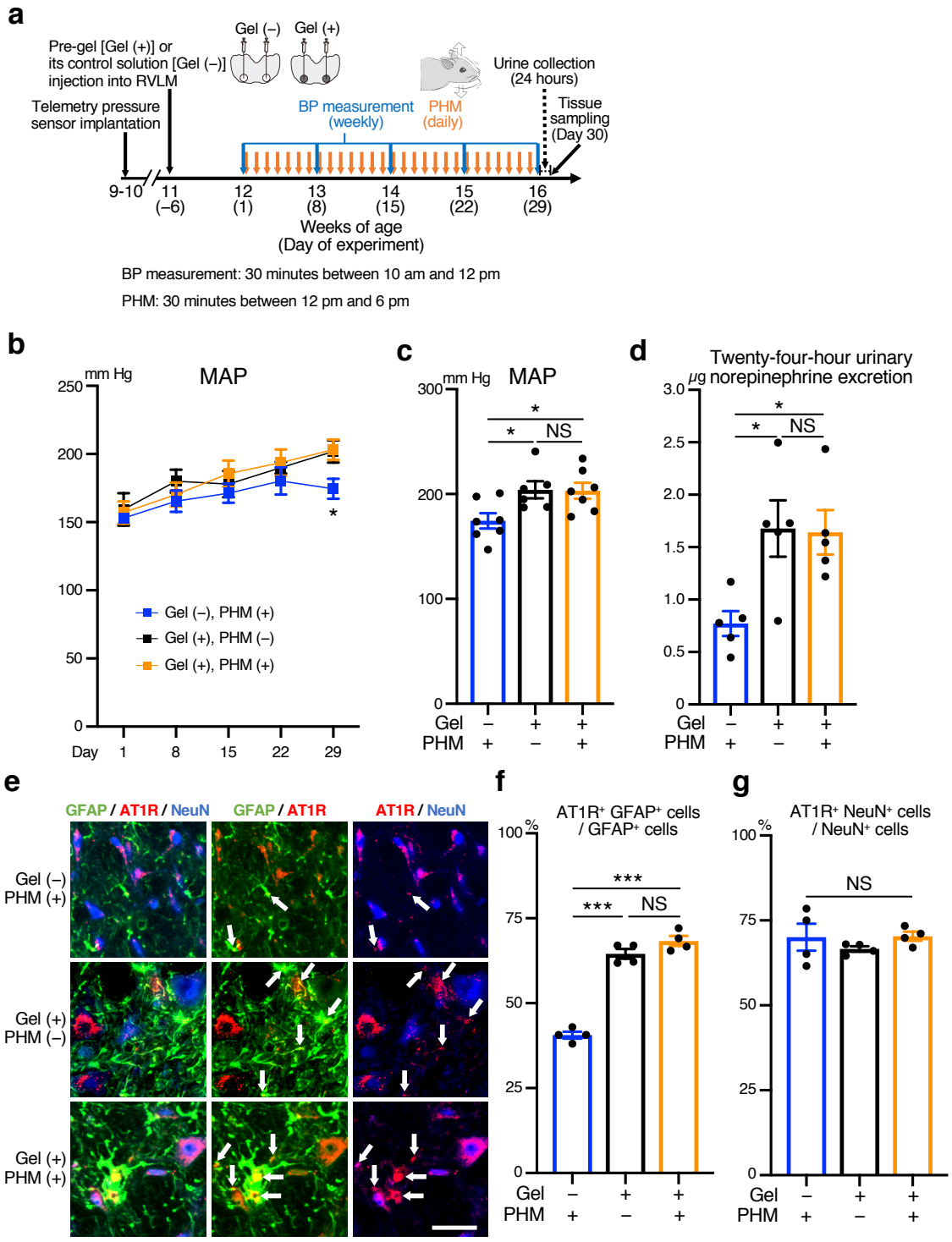

752

753 **Fig. 6 | Hydrogel introduction eliminates decreasing effects of PHM on BP and AT1R**

754 **expression in the RVLM astrocytes in SHRSPs. a,** Schematic representation of experimental

755 protocol for analysis of the effects of PHM with and without PEG hydrogel introduction in bilateral
756 RVLMs of SHRSPs. PHM was applied daily for consecutive 28 days. **b−d,** Time courses **(b)** and
757 values on Day 29 **(c)** of MAP, and 24-hour urinary norepinephrine excretion **(d)** of SHRSPs,
758 subjected to various combinations of daily PHM application and hydrogel introduction in bilateral
759 RVLMs. Note the absence of significant difference in BP **(b,c)** and urinary norepinephrine excretion
760 **(d)** of SHRSPs with hydrogel introduced RVLMs [Gel (+)] between with and without PHM [**b**: P =
761 0.0372 for Day 29. **c**: P = 0.0387 for column 1 vs. 2, P = 0.0372 for column 1 vs. 3, and P = 0.9959
762 for column 2 vs. 3. n = 7 rats for Gel (−), PHM (+) and for Gel (+), PHM (+); n = 6 rats for Gel (+),
763 PHM (−); **d**: P = 0.0247 for column 1 vs. 2, P = 0.0307 for column 1 vs. 3, and P = 0.9920 for
764 column 2 vs. 3. n = 5 rats for each group]. **e**, Micrographic images of anti-GFAP (green), anti-AT1R
765 (red), and anti-NeuN (blue) immunostaining of the RVLM in SHRSPs subjected to various
766 combinations of hydrogel introduction in bilateral RVLMs and 4-week PHM application. Arrows
767 point to anti-AT1R immunosignals that overlap with anti-GFAP, but not anti-NeuN, immunosignals
768 in merged images. Scale bar, 50 μm. Images are representative of four rats. **f,g,** Quantification of
769 AT1R-positive astrocytes **(f)** and neurons **(g)** in the RVLM. Note the absence of significant
770 difference in the ratio of AT1R-positive astrocytes of SHRSPs with hydrogel introduced RVLMs
771 [Gel (+)] between with and without PHM (**f**, columns 2 and 3). Fifty $NeuN^+$ cells and one hundred
772 $GFAP^+$ cells were analyzed for each rat (**f**: $P < 0.0001$ for column 1 vs. 2, $P < 0.0001$ for column 1

773 vs. 3, and $P = 0.1597$ for column 2 vs. 3. **g**: $P = 0.5182$. $n = 4$ rats for each group). Data are

774 presented as mean ± s.e.m. *$P < 0.05$; ***$P < 0.001$; NS, not significant, one-way ANOVA with

775 Tukey's post hoc multiple comparisons test.

Extended Data Fig. 4

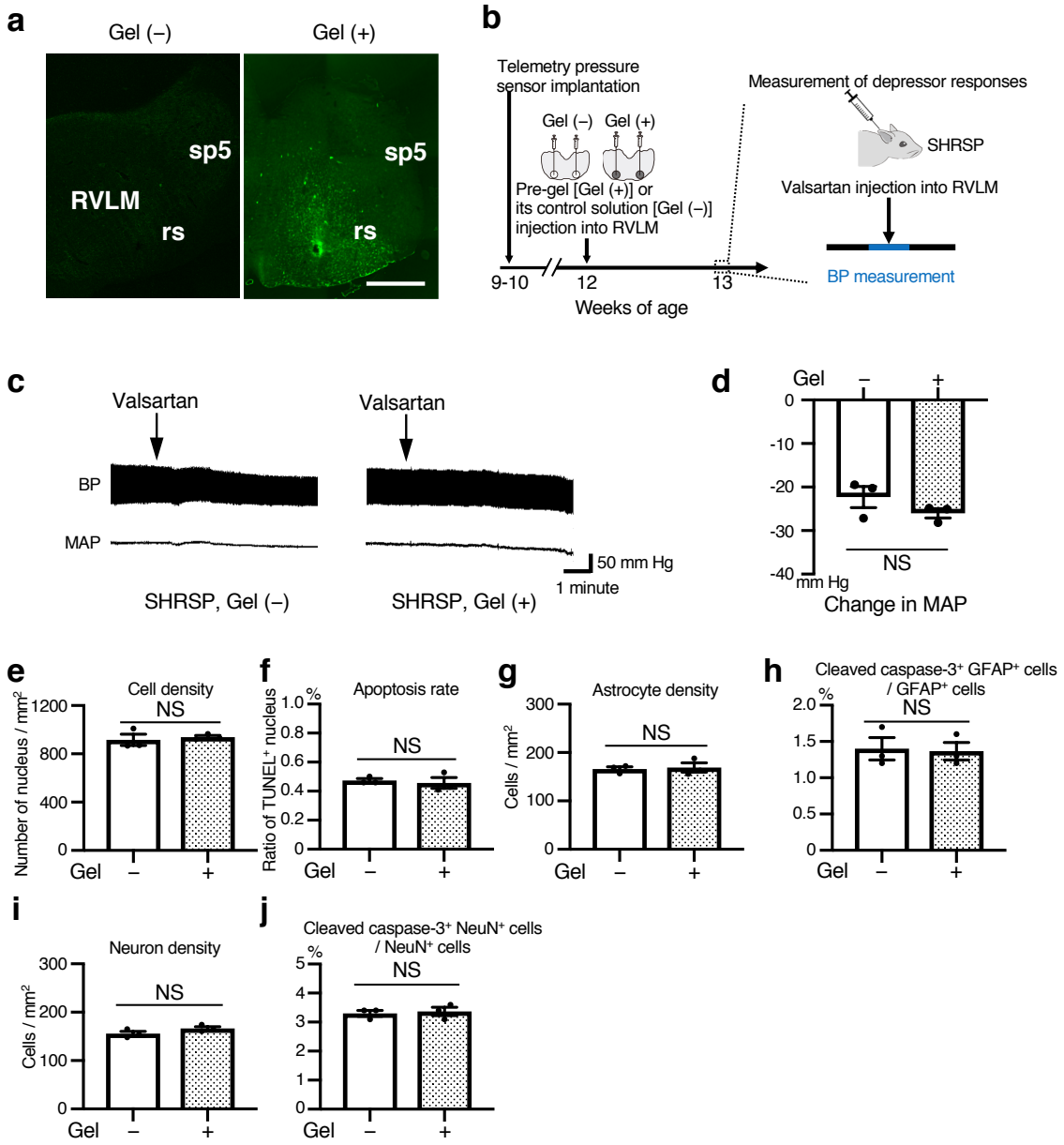

Extended Data Fig. 4 | Hydrogel introduction in the RVLM does not affect the depressor response to valsartan or survival/apoptosis of RVLM astrocytes and neurons in SHRSPs. a, Introduction of PEG hydrogel in rat RVLM. Twenty-four hours after the injection of control ungelatable fluorescent PEG solution (left) or 1 week after the injection of pre-gel fluorescent PEG

781 solution (right), brainstem samples were prepared. Coronal-section images representative of three
782 rats with similar results are shown. Scale bar, 1 mm. **b,** Schematic representation of experimental
783 protocol. One week after the injection of pre-gel PEG solution or its ungelatable control, depressor
784 response was analyzed as in Fig. 2. **c,d,** Representative trajectories **(c)** and quantification **(d)** of BP
785 descent upon valsartan injection to the RVLM of SHRSPs with or without hydrogel introduction (**d**:
786 $P = 0.2342$. $n = 3$ rats for each group). **e−j,** Effects of hydrogel introduction on survival/apoptosis
787 of RVLM cells in SHRSPs. Rat RVLM sections prepared in the experiments for Fig. 6e−g [PHM
788 (+), Gel (−) and PHM (+), Gel (−)] were subjected to TUNEL assay **(e,f)**, or combinations of anti-
789 GFAP, anti-NeuN and anti-cleaved caspase-3 immunostaining **(g−j)**. DAPI-positive nuclei **(e)**,
790 GFAP- **(g)** or NeuN- **(i)** positive cells were counted, and the relative populations of cells doubly
791 positive for indicated combinations of TUNEL **(f)** and cleaved caspase-3 **(h,j)** were quantified. Each
792 value represents an average from five images of 1 x 1-mm area analyzed for each rat (**e**: $P = 0.6518$.
793 **f**: $P = 0.6943$. **g**: $P = 0.7938$. **h**: $P = 0.8722$. **i**: $P = 0.1679$. **j**: $P = 0.7247$. $n = 3$ rats for each group).
794 Data are presented as mean ± s.e.m. NS, not significant; unpaired two-tailed Student's *t*-test.

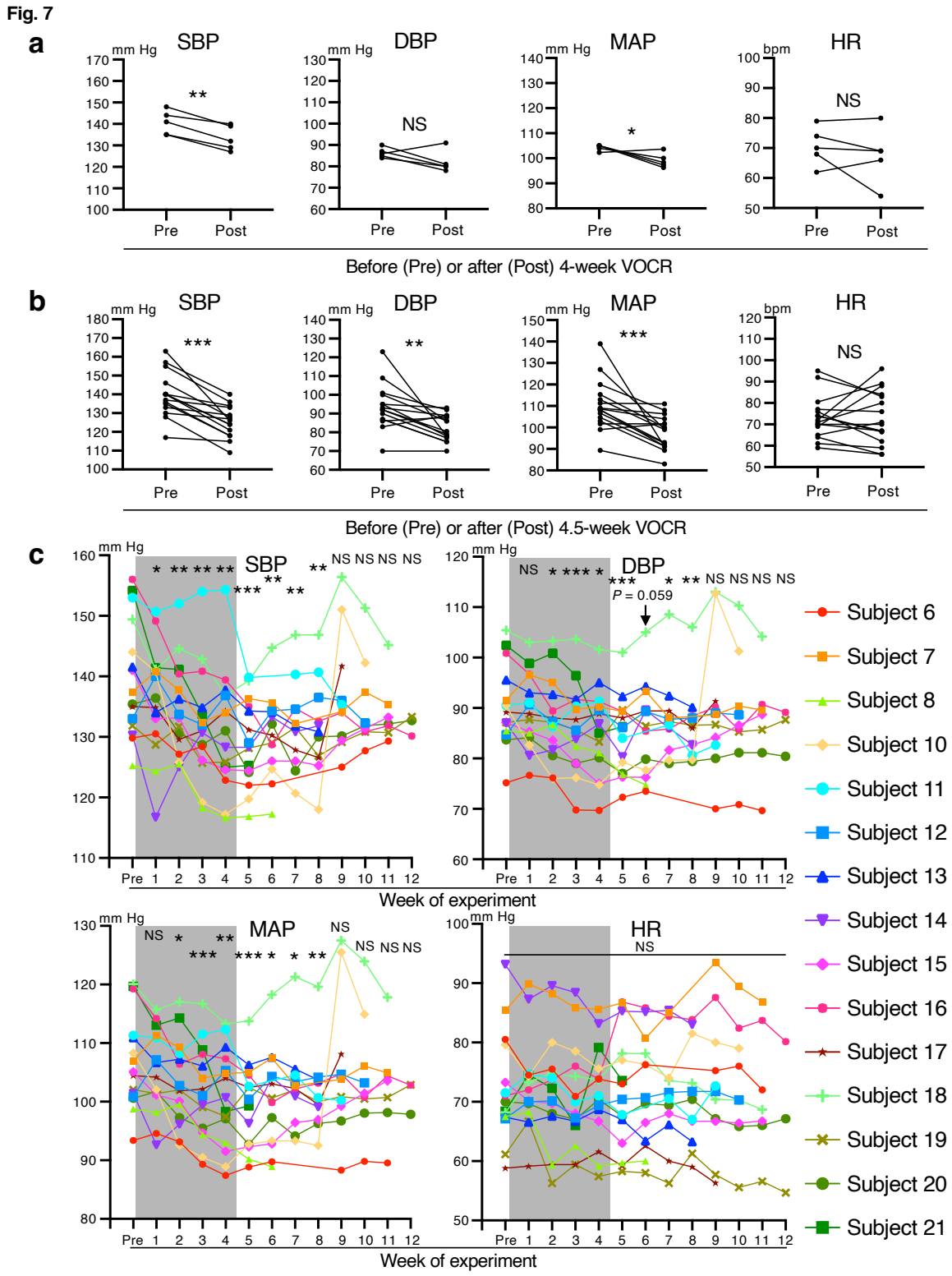

Fig. 7 | VOCR has an antihypertensive effect on hypertensive adult humans. a, BP and HR

797 “value of the day”s immediately before and after 4-week VOCR in the study of protocol 1 (SBP: P

798 = 0.0018. DBP: P = 0.1509. MAP: P = 0.0459. HR: P = 0.3900. n = 5). **b,** BP and HR “value of the

799 week”s immediately before and after 4.5-week VOCR in the study of protocol 2 (SBP: P < 0.0001.

800 DBP: P = 0.0031. MAP: P = 0.0009. HR: P = 0.9817. n = 15). **c,** Subject number-corresponding

801 trajectories and statistical analysis of BP and HR in the study of protocol 2. Gray-shaded rectangles

802 indicate the VOCR intervention periods (4.5 weeks). The colors and symbols of individual lines

803 correspond to those of individual subject numbers listed on the right, excluding subject 9 (see

804 Supplementary Table 2). Each “value of the week” was statistically compared with that of the week

805 immediately before the initiation of VOCR intervention (SBP: P = 0.0293 for Pre vs. Week 1, P =

806 0.00228 for Pre vs. Week 2, P = 0.0013 for Pre vs. Week 3, P = 0.0035 for Pre vs. Week 4, P =

807 0.0002 for Pre vs. Week 5, P = 0.0078 for Pre vs. Week 6, P = 0.0035 for Pre vs. Week 7, P =

808 0.0075 for Pre vs. Week 8, P = 0.2132 for Pre vs. Week 9, P = 0.1314 for Pre vs. Week 10, P =

809 0.0973 for Pre vs. Week 11, and P = 0.3993 for Pre vs. Week 12. DBP: P = 0.3022 for Pre vs. Week

810 1, P = 0.0436 for Pre vs. Week 2, P = 0.0010 for Pre vs. Week 3, P = 0.0100 for Pre vs. Week 4, P =

811 0.0006 for Pre vs. Week 5, P = 0.0599 for Pre vs. Week 6, P = 0.0488 for Pre vs. Week 7, P =

812 0.0096 for Pre vs. Week 8, P = 0.9346 for Pre vs. Week 9, P = 0.7850 for Pre vs. Week 10, P =

813 0.0769 for Pre vs. Week 11, and P = 0.3137 for Pre vs. Week 12. MAP: P = 0.1075 for Pre vs. Week

814 1, P = 0.0132 for Pre vs. Week 2, P = 0.0008 for Pre vs. Week 3, P = 0.0063 for Pre vs. Week 4, P =

0.0003 for Pre vs. Week 5, $P = 0.0251$ for Pre vs. Week 6, $P = 0.0136$ for Pre vs. Week 7, $P = 0.0071$ for Pre vs. Week 8, $P = 0.6795$ for Pre vs. Week 9, $P = 0.4295$ for Pre vs. Week 10, $P = 0.0704$ for Pre vs. Week 11, and $P = 0.3662$ for Pre vs. Week 12. HR: $P = 0.6287$ for Pre vs. Week 1, $P = 0.7840$ for Pre vs. Week 2, $P = 0.1573$ for Pre vs. Week 3, $P = 0.5380$ for Pre vs. Week 4, $P = 0.7331$ for Pre vs. Week 5, $P = 0.6995$ for Pre vs. Week 6, $P = 0.9110$ for Pre vs. Week 7, $P = 0.9875$ for Pre vs. Week 8, $P = 0.5866$ for Pre vs. Week 9, $P = 0.9566$ for Pre vs. Week 10, $P = 0.6487$ for Pre vs. Week 11, and $P = 0.9905$ for Pre vs. Week 12. $n = 15$ for Pre and Weeks 1 to 5, $n = 13$ for Week 6, $n = 12$ for Week 7, $n = 11$ for Weeks 8 and 9, $n = 9$ for Week 10, $n = 7$ for Week 11, $n = 3$ for Week 12). *$P < 0.05$; **$P < 0.01$; ***$P < 0.001$; NS, not significant, paired two-tailed Student's *t*-test.

Extended Data Fig. 5

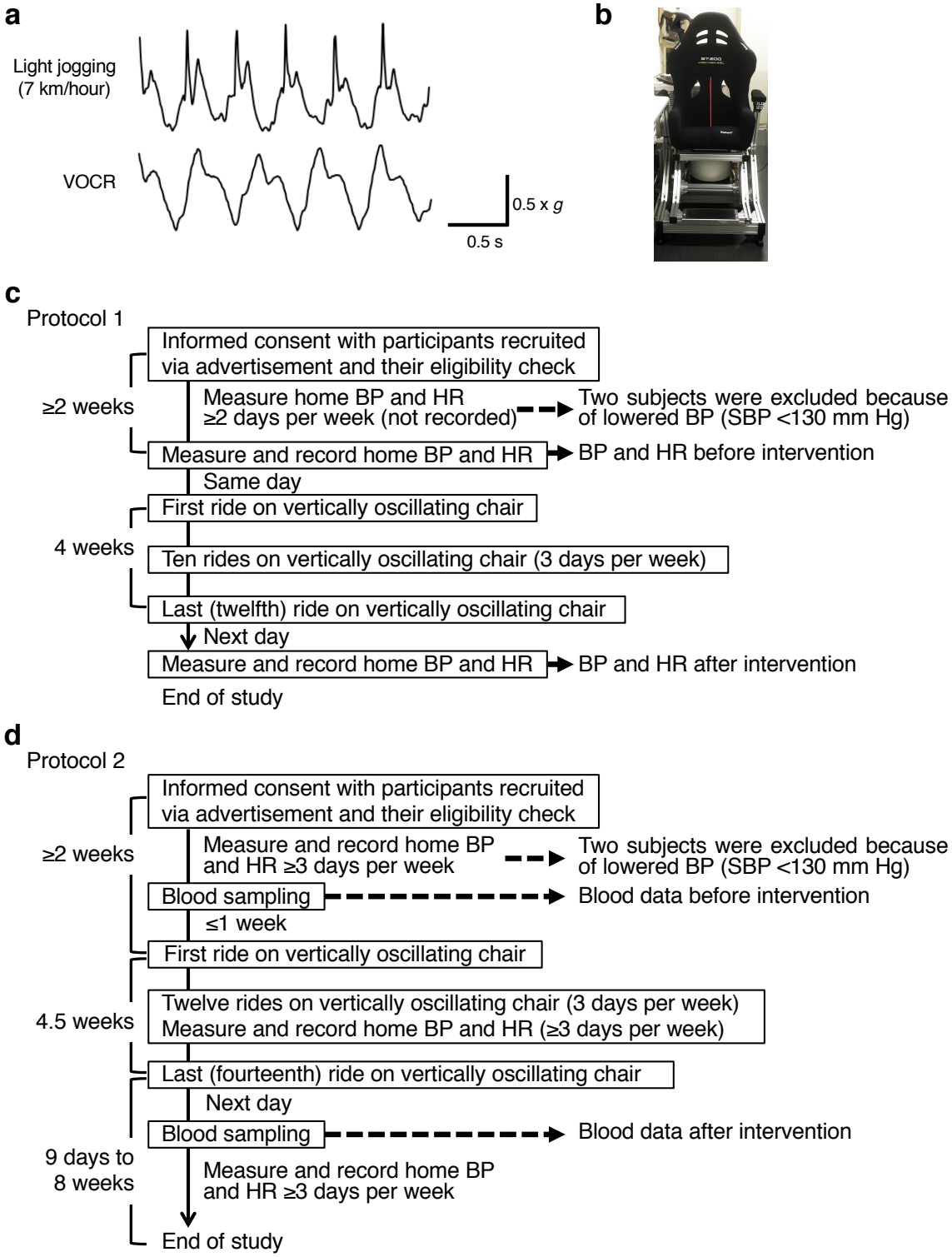

Extended Data Fig. 5 | Vertically oscillating chair that reproduces mechanical impacts on the

827 **head during light jogging, and protocols of clinical study to examine antihypertensive effect of**

828 **VOCR on hypertensive adult humans. a,** Vertical accelerations generated at adult human head

829 during light jogging on a treadmill machine (velocity: 7 km/hour) and VOCR (frequency: 2 Hz).

830 The VOCR system was adjusted to produce ~1.0 x *g* vertical acceleration peaks. Right-angled scale

831 bar, 0.5 x *g* / 0.5 s. Images are representative of three independent experiments with similar results.

832 **b**, Photograph of the chair. **c,d,** Protocol 1 **(c)** and 2 **(d)**.

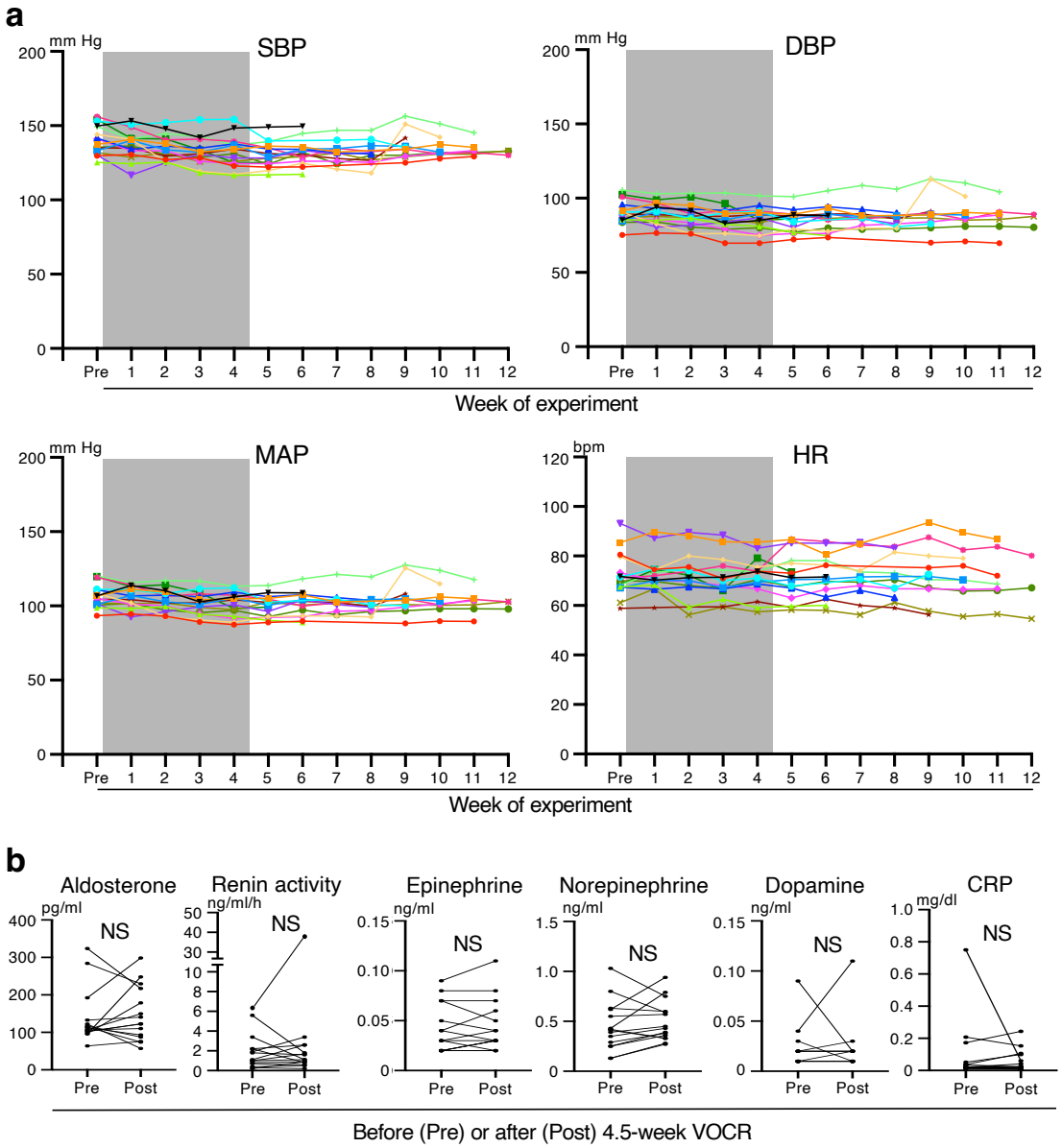

Extended Data Fig. 6 | Trajectories of BP and HR, and blood test values before and after the intervention period in the study of protocol 2. a, Trajectories of "value of the week"s of BP and HR. Gray-shaded rectangles indicate the VOCR intervention periods. The colors and symbols of individual lines correspond to those of individual subjects (Fig. 7c). The black line with inverted triangles indicates subject 9. **b,** Blood test values before and after the intervention period.

839 Significant change was not observed in any of tested parameters. NS, not significant; paired two-
840 tailed Student's *t*-test. (Aldosterone: $P = 0.6265$. Renin activity: $P = 0.3794$. Epinephrine: $P =$
841 0.5103. Norepinephrine: $P = 0.2653$. Dopamine: $P > 0.9999$. CRP: $P = 0.4412$.). A participant
842 (subject 18) showed a large increase in plasma renin activity after VOCR. We advised him to
843 consult his primary care physician, who ruled out the disqualifying conditions for this study (e.g.,
844 severe renal disease; see Methods) based on comprehensive evaluation. Therefore, we did not
845 exclude subject 18 from our statistical analysis of BP and HR.

Supplementary Table 2

Subject #	Sex Age (years) Body weight (kg) Height (cm) BMI	Period since diagnosis or self-recognition as hypertension Health problems and diseases other than hypertension	Smoking Alcohol (if yes, how often)	Current medication (dose per day)	Habitual exercise (times per week)	SBP/DBP (mm Hg) and HR (bpm) just before (left) and after (right) VOCR period (month of first - last bout of VOCR)	
1	Male 60 73 165.2 27.2	13 years Hyperuricemia	No Almost every day	Azilsartan・Amlodin (20 mg・5 mg) Febuxostat (10 mg) Bisoprolol fumarate (5 mg)	Walking 90 minutes (3 or 4 times)	148/85 62 February - March	139/78 66
2	Female 53 50 159 19.8	14 years None	No Almost every day	None	Sit-ups 2 x 30 times (every day)	135/90 70 March	127/81 69
3	Male 37 113 186 32.7	19 years None	No Occasionally	None	Judo (once)	135/86 68 March	129/91 54
4	Female 60 73 156 30	6 years None	No Occasionally	None	None	141/87 79 April - May	132/80 80
5	Female 52 50 148 22.8	1 year None	No Occasionally	Azilsartan (20 mg) Amlodin (2.5 mg)	None	144/84 74 April - May	140/80 69
6	Female 57 68 164 25.3	10 years None	No Occasionally	None	None	128/70 77 November - December	109/70 76
7	Male 61 67 168 23.7	Uncertain (<1 year) Diabetes mellitus Hyperlipidemia	No No	Metformin hydrochloride (1000 mg) Rosuvastatin calcium (5 mg) Sitagliptin phosphate hydrate (50 mg)	Walking 120 minutes (once)	146/100 92 November - December	128/86 84
8	Male 46 72 178 22.7	3 months Allergic rhinitis	Yes Occasionally	Montelukast sodium (10 mg) Ebastine (10 mg)	Walking 60 minutes (once) Stretching 30 minutes (once)	135/95 61 November - December	118/78 59
9	Male 55 87 173 29.1	7 months Diabetes mellitus	No No	None	Karate (2 or 3 times)	156/89 74 November - December	145/94 67
10	Male 70 62 166 22.5	6 months None	No Occasionally	None	Walking 40 minutes (4 times)	140/92 81 November - December	121/79 89
11	Female 60 45 157 18.3	Uncertain (>1year) Breast cancer (post-surgery)	No Almost every day	Tamoxifen citrate (20 mg)	None	155/92 74 November - December	136/81 67
12	Male 68 72 171 24.6	Uncertain (<1 year) None	No No	None	None	133/86 70 January - February	129/88 70
13	Female 56 58 160 22.7	7 years None	No No	Telmisartan・Amlodipine (40 mg・5 mg)	None	137/95 65 January - February	133/93 71
14	Male 49 69 168 24.5	Uncertain (<1 year) Diabetes mellitus	No No	Sitagliptin phosphate hydrate (50 mg) Acetazolamide (250 mg)	None	140/90 95 January - February	124/77 83

Subject #	Sex Age (years) Body weight (kg) Height (cm) BMI	Period since diagnosis or self-recognition as hypertension Health problems and diseases other than hypertension	Smoking Alcohol (if yes, how often)	Current medication (dose per day)	Habitual exercise (times per week)	SBP/DBP (mm Hg) and HR (bpm) just before (left) and after (right) VOCR period (month of first - last bout of VOCR)	
15	Male 43 69 165 25.3	Uncertain (<1 year) None	No Occasionally	None	None	140/87 76 August - September	124/75 62
16	Female 48 45.3 157.2 18.3	15 years None	No Occasionally	None	Walking 60 minutes (6 times)	157/101 72 October - November	140/92 96
17	Male 65 60.1 167.1 21.5	8 years None	Yes Almost every day	None	None	140/93 59 October	134/89 56
18	Male 55 93.4 168.1 33.1	8 years Reflex esophagitis Hyperlipidemia	No Almost every day	Azilsartan (20 mg) Lansoprazole (15 mg) Atorvastatin calcium hydrate (10 mg) Benidipine hydrochloride (4 mg)	None	172/123 69 November - December	115/78 88
19	Male 41 92.3 183.2 27.5	2 years None	No Almost every day	None	Walking 60 minutes (3 times)	130/83 64 January - February	127/89 56
20	Female 65 48.7 158.6 19.4	1 year Hyperlipidemia Lumbar spinal canal stenosis (post-surgery)	No Almost every day	Amlodipine besilate (5 mg) Atorvastatin calcium hydrate (10 mg) Limaprost alfadex (15 μg) Loxoprofen sodium hydrate (120 mg) Rebamipide (200 mg)	Swimming 40 minutes (5 times)	136/87 70 January - February	118/75 67
21	Male 32 65.1 168.9 22.8	2 years None	No Almost every day	None	None	163/109 71 January - February	126/86 80

Supplementary Table 2 | Information of subjects who participated in the human studies. Subjects 1−5 were participants in the study of protocol 1, and subjects 6−21 participated in the study of protocol 2. Subject 9 was excluded from our statistical analysis because of high serum CRP value before VOCR (2.85 mg/dL), which made it difficult to rule out acute infection, a possible disqualifier, at the time of initiation of VOCR, albeit the lack of specific complaint or local symptom related to acute physical problem(s). His serum CRP after the VOCR period was within the normal range (0.12 mg/dL).

Extended Data Fig. 7

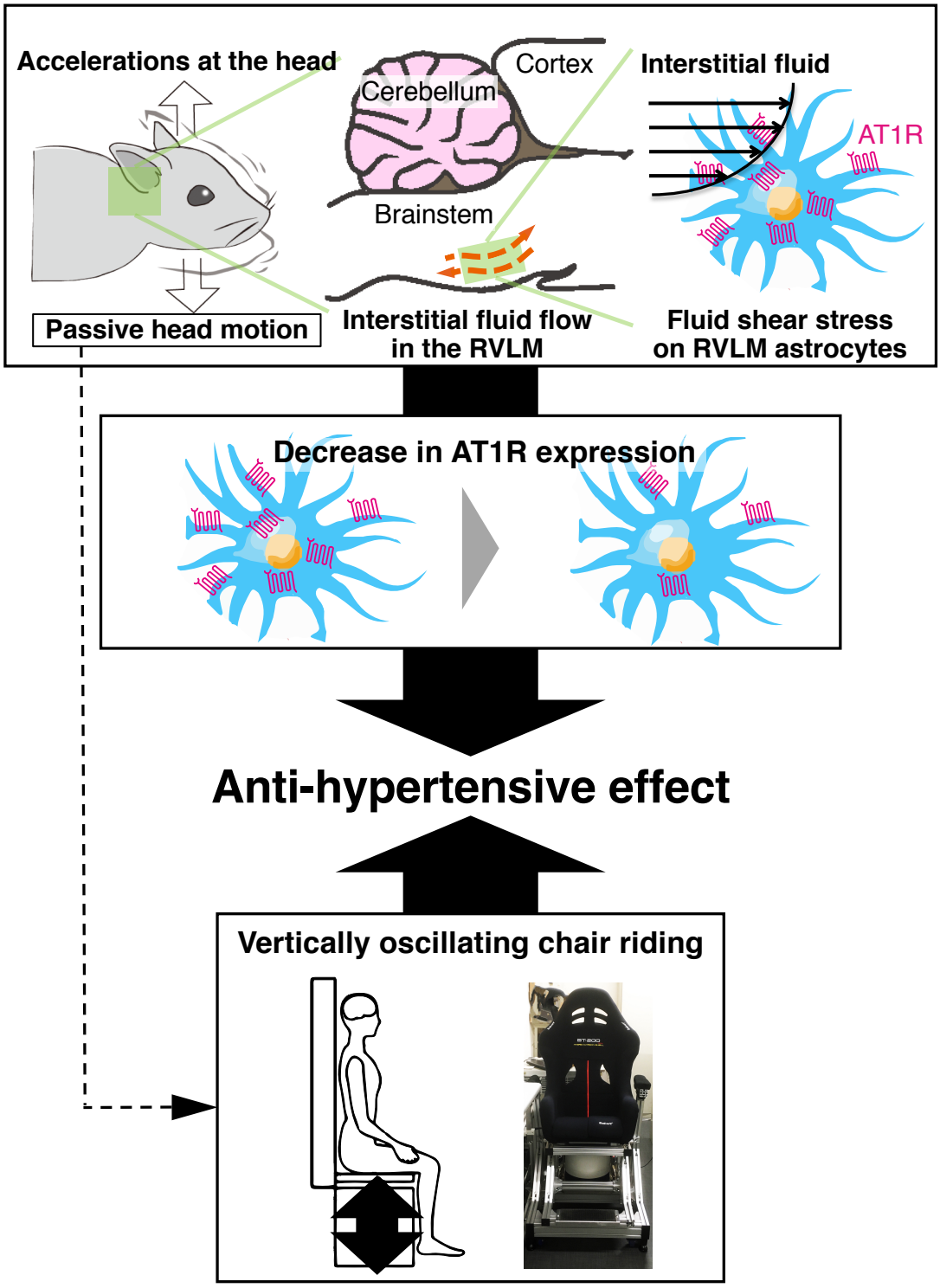

857

858 **Extended Data Fig. 7 | Schematic representation of the antihypertensive effects observed in**

859 **PHM of hypertensive rats and VOCR of hypertensive humans.** The results from our animal
860 experiments indicate that cyclical mechanical impact on the head generates interstitial fluid
861 movement in the RVLM, leading to FSS-induced decrease in AT1R expression in astrocytes in situ,
862 and thereby ameliorates hypertension. Our studies also show that the VOCR of hypertensive adult
863 humans, which produces vertical accelerations at their heads, lowers their BP.

Methods

Animal experiments and human studies. Animals were housed under a 12/12 hour light-dark cycle with controlled temperature (23−25°C), and treated with humane care under approval from the Animal Care and Use Committee of National Rehabilitation Center for Persons with Disabilities (approval number: 30-07). Male SHRSP/Izm and WKY/Izm rats were provided from the Disease Model Cooperative Association (Kyoto, Japan) and astrocyte-GFP mice (Aldh1L1-GFP mice)[37] were obtained from GENSAT (New York, NY), acclimated to the laboratory environments for at least 1 week, randomly divided into experimental groups, and used for experiments.

All participants in our human studies provided written informed consent. The studies were approved by the Ethics Committees of the Iwai Medical Foundation and the National Rehabilitation Center for Persons with Disabilities (approval number: 30-01).

Chemicals and antibodies. All the chemicals were purchased from Sigma-Aldrich unless noted otherwise. Primary antibodies and their dilution rates used in this study are as follows: mouse monoclonal anti-GFAP (MAB360; Millipore, Billerica, MA) at 1:1,000; rabbit polyclonal anti-GFAP (Z0334; Dako, Glostrup, Denmark) at 1:1,000; chicken polyclonal anti-GFAP (ab4674; Abcam, Cambridge, UK) at 1:2,000; rabbit polyclonal anti-cleaved caspase-3 (9661; Cell Signaling Technology, Danvers, MA) at 1:1,000; mouse monoclonal anti-NeuN (MAB377; Millipore) at

882 1:200; rabbit polyclonal anti-NeuN (ABN78; Millipore) at 1:1,000, rabbit polyclonal anti-AT1R
883 (HPA003596; Sigma-Aldrich, St. Louis, MO) at 1:200; rabbit polyclonal anti-AGTRAP
884 (HPA044120; Sigma-Aldrich) at 1:1000; rabbit polyclonal anti-GFP (598; MBL, Nagoya, Japan) at
885 1:2,000; chicken polyclonal anti-GFP (ab13970; Abcam) at 1:2,000; mouse monoclonal anti-TUJ-1
886 (ab78078; Abcam) at 1:1000. Secondary antibodies conjugated with Alexa Fluor 350, 488, 568,
887 633, and 647 (Thermo Fisher Scientific, Waltham, MA) were used at the dilution rate of 1:400. Cell
888 nuclei were stained with DAPI (D9542; Sigma-Aldrich).
889
890 **PHM application to rats.** Rats were subjected to PHM in a prone position using a platform that we
891 developed to move their heads up and down[24] (schematically represented in Fig. 1a). During PHM,
892 animals were kept anesthetized with 1.5% isoflurane except for the μCT study, in which we used
893 intraperitoneal injection of 2 mg/kg of midazolam (Sandoz, Basel, Switzerland), 2.5 mg/kg of
894 butorphanol (Meiji Seika, Tokyo, Japan) and 0.15 mg/kg of medetomidine (Kyoritsu Seiyaku,
895 Tokyo, Japan) for anesthesia. Body temperature of tested animals was maintained using a light
896 heater. The PHM system was set up to reproduce the head motion (5 mm, 2 Hz) of treadmill
897 running (20 m/minute) which made 1.0 x *g* vertical acceleration peaks at the head of rats
898 examined[24]. The control rats in PHM experiments were anesthetized likewise, and placed in a prone
899 position with their heads on the platform that was left static.

900

901 **Treadmill running of rats.** Rats were subjected to compulsive running using a belt drive treadmill
902 equipped with an electrical shock system (MK-680S; Muromachi, Tokyo, Japan). We habituated the
903 rats to the treadmill system by placing them in the machine several times without turning on the
904 treadmill belt during the acclimation period. The electrical stimulation was turned on only once or
905 twice during the first 5 minutes of the 30-minute treadmill running on the first day of the 4-week
906 treadmill running period. Thereafter, we did not need to turn on the electrical shock system to have
907 the animals keep running, perhaps because the velocities we employed (20 m/minute) were
908 moderate. The control rats in treadmill running experiments were placed on the belt daily for 30
909 minutes without turning on the treadmilling.

910

911 **Measurement of BP and HR of rats by radio-telemetry.** Rats were implanted with a telemetry
912 pressure probe (Millar, Houston, TX) in the abdominal aorta at 9−10 weeks of age, following the
913 surgical procedure described previously[61]. Rats were allowed to recover for at least 14 days before
914 the initiation of experimental interventions or analyses. During the periods of experimentation that
915 involved repeated BP and HR measurements over multiple weeks, BP and HR were monitored and
916 recorded for continuous 30 minutes every 7 days between 10:00 AM and 12:00 PM (noon) by a
917 multichannel amplifier and signal converter (LabChart 8; ADInstruments, Dunedin, New Zealand).

918 Mean arterial pressure (MAP) was calculated with a standard formula as follows: MAP = diastolic
919 BP (DBP) + 1/3 [systolic BP (SBP) – DBP].
920
921 **Measurement of urinary norepinephrine excretion of rats.** Urine excreted during the indicated
922 24-hour period was collected by means of a metabolic cage (KN-646; Natsume Seisakusho, Tokyo,
923 Japan), and stored at −80˚C until assayed. Excretion of urinary norepinephrine was calculated by
924 multiplying its concentration measured using an enzyme-linked immunosorbent assay (ELISA) kit
925 (KA1891; Abnova, Taipei, Taiwan) with the urine volume.
926
927 **Microinjection into rat RVLM.** Rats were anesthetized with intraperitoneal injection of
928 midazolam, butorphanol, and medetomidine except for Ang II or valsartan injection studies, in
929 which we used 1.2−1.4 g/kg of urethane (Sigma-Aldrich), and subjected to microinjection as
930 described previously[62]. In brief, a 25s-G microsyringe (Hamilton, Bonaduz, Switzerland) was
931 stereotaxically positioned on anesthetized rats after exposure of dorsal surface of medulla. The
932 needle placement was defined according to an atlas of the rat with stereotaxic coordinates[63];
933 anteroposterior angle: 18˚, 1.8 mm lateral to the calamus scriptorius, 3.5 mm ventral to the dorsal
934 surface of the medulla. The placement of the needle tip in RVLM was confirmed by ensuring the
935 pressure response to a test-dose injection of L-glutamate[12,64] (100 nL of 1 mmol/L in PBS).

936 Microinjection of various compounds or mediums was made through a needle reinserted at the
937 same coordinates with fixed infusion rates using a microsyringe pump instrument (KD scientific,
938 Holliston, MA). Except for experiments to analyze pressor or depressor responses, we held the
939 syringe for 5 minutes after the injection to avoid reflux, pulled out the needle carefully, and sutured
940 the skin. The volumes and rates of microinjection were as follows; Ang II (Auspep, Tullamarine,
941 Australia) and valsartan (Tocris Bioscience, Bristol, UK): 100 nL of 1 mmol/L in PBS at 0.1
942 μL/minute, AAV solutions: 300 nL at 0.03 μL/minute, PEG solutions: 1 μL at 0.1 μL/minute,
943 Isovist: 1 μL at 0.2 μL/minute.
944
945 **Analysis of pressor/depressor responses.** Rats implanted with a telemetry pressure probe were
946 anesthetized with urethane, and subjected to the analysis of pressor/depressor responses. Monitoring
947 the BP, we injected Ang II or valsartan (100 pmol) stereotaxically into the unilateral RVLM
948 following the microinjection procedures described above. The injection side (right or left) was
949 chosen randomly. When both pressor and depressor responses were analyzed, at least 2 hours
950 elapsed between the injections of Ang II and valsartan (Fig. 2a). The maximal MAP change elicited
951 from the baseline was statistically analyzed[14].
952
953 **Production of AAV vectors.** To obtain astrocyte- and neuron-specific transduction, we used AAV9

954 vectors that expressed a transgene under the control of mouse GFAP and rat NSE promoters,
955 respectively. The astrocyte-specific GFAP promoter consists of 0.6-kb hybrid fragments containing
956 ABC1D genomic regions upstream of the mouse *GFAP* gene[65]. The neuron-specific NSE promoter
957 is composed of the 1.2-kb genomic region upstream of the rat *NSE* gene[66]. Full-length rat AGTRAP
958 cDNA was synthesized (Eurofins Genomics, Tokyo, Japan) and inserted into plasmid pAAV-GFAP-
959 GFP-P2A-Cre-woodchuck hepatitis virus post-transcriptional regulatory element (WPRE)-simian
960 virus 40 polyadenylation signal (SV40pA) and pAAV-NSE-GFP-P2A-Cre-WPRE-SV40pA to
961 generate pAAV-GFAP-GFP-P2A-AGTRAP-WPRE-SV40pA and pAAV-NSE-GFP-P2A-
962 AGTRAP-WPRE-SV40pA. pAAV-GFAP-GFP-WPRE-SV40pA and pAAV-NSE-GFP-WPRE-
963 SV40pA were used for experimental controls. Recombinant single-strand AAV2/9 vectors were
964 produced by transfection of HEK293T cells (Thermo Fisher Scientific) with the respective pAAV
965 expression plasmid, pAAV2/9 and a helper plasmid (Stratagene, La Jolla, CA) as previously
966 described[67]. After harvesting conditioned medium, the viral particles were precipitated using
967 polyethylene glycol 8000 and iodixanol continuous gradient centrifugation as previously
968 described[68]. The genomic titer of purified AAV9 vectors was determined by qPCR that targeted the
969 WPRE sequence.
970
971 **Measurement of pressure in rat RVLM.** Intra-brainstem pressure (IBP) was measured using a

972 blood pressure telemeter by means of the procedure we previously reported[24,69]. The pressure sensor
973 was placed in rat RVLM using the same approach with the microinjection described above. During
974 IBP measurement, respiration was monitored using a respiration sensor attached to the tested rats.
975 Low-pass (50 Hz) filtered IBP waves were analyzed using LabChart 8 software (ADInstruments).
976 We observed ~0.5-Hz respiration-synchronized IBP changes with ~2.5 mm Hg magnitude (peak to
977 peak) as well as 2-Hz PHM-specific waves with ~1.2 mm Hg magnitude (peak to peak).
978
979 **In vivo analysis of the distribution dynamics of interstitial fluid in rat RVLM using μCT.**
980 Isovist (Bayer, Berlin, Germany) was stereotaxically microinjected into RVLM of anesthetized 12-
981 week-old male WKY rats following the procedure described above, and visualized using μCT
982 (inspeXio SMX-100CT, Shimadzu, Kyoto, Japan). After Isovist injection, rats were subjected to
983 two serial brain μCT scans between which PHM was either applied or left unapplied (kept
984 sedentary) for 30 minutes (Fig. 4e). μCT images were analyzed using software for 3D morphometry
985 (TRI/3D-BON-FCS64, RATOC System, Tokyo, Japan). Voxels with ≥1.02 times signal intensity as
986 compared with that of air was defined as Isovist cluster in rat RVLM.
987
988 **Simulative calculation of the magnitude of FSS on the cells in rat RVLM during PHM.** We
989 calculated interstitial fluid flow-derived FSS imposed on cells in rat RVLM by referring the results

990 from our μCT analysis (Fig. 4g,h) to the Henry Darcy's law, which defines the flux density of
991 penetrating fluid per unit time[70]). The velocity of interstitial fluid flow (u) is assumed to approach
992 the superficial velocity (u_∞) and zero (u=0) at the cell surface (i.e., a no-slip condition). Using these
993 two boundary conditions together with the Brinkman equation, FSS (τ) at the interstitial cell surface
994 can be obtained as described in Supplementary Table 1[60].
995
996 **Cell culture.** Primary cultures of astrocytes were prepared from the cortex of neonatal (2−3 days
997 old) astrocyte-GFP mouse[37] pups by physical dissociation as previously described[71]. Cells were
998 maintained in DMEM/F12 supplemented with 10% FBS (GE Healthcare Life Science,
999 Marlborough, MA), 100 I. U./mL penicillin and 100 μg/mL streptomycin at 37°C in a humidified
1000 incubator (5% CO_2 and 95% air). Culture medium was replaced with fresh one every 3−4 days until
1001 confluent. Astrocytes were detached with trypsin/EDTA (0.05% trypsin, 0.53 mM EDTA in PBS),
1002 replated at a ratio of 1:10, and grown to approximately 80−90% confluence prior to use.
1003 Mouse neuroblastoma-derived Neuro2A cells (provided from Dr. Yokota, Tokyo Medical and
1004 Dental University, Japan), which exhibit neuronal phenotypes and morphology[39,40], were cultured in
1005 DMEM (Wako, Japan) supplemented with 10% FBS, 100 I. U./mL penicillin and 100 μg/mL
1006 streptomycin at 37°C in a 5% CO_2 incubator.
1007

1008 **Application of FSS to astrocytes or Neuro2A cells in culture.** Astrocytes or Neuro2A cells grown
1009 in a poly-D-lysine-coated 35-mm culture dish (Corning Life Sciences, Corning, NY) were exposed
1010 to pulsatile FSS (average 0.7 Pa) for 30 minutes. As we previously reported[23,24,35], a parallel plate
1011 flow-chamber and a roller pump (Masterflex; Cole-Parmer, Vernon Hills, IL) were used to apply
1012 FSS. The flow-chamber, which was composed of a cell culture dish, a polycarbonate I/O unit, and a
1013 silicone gasket, generated a 23-mm-long 10-mm-wide 0.5-mm-high flow channel. To maintain pH
1014 and temperature of culture medium, we used a 5% CO_2-containing reservoir and a temperature-
1015 controlled bath.
1016
1017 **Tissue preparation and immunostaining (immunohistochemical or immunocytochemical**
1018 **analysis).** Rats were anesthetized with intraperitoneal injection of midazolam, butorphanol, and
1019 medetomidine, and perfused transcardially with 4% paraformaldehyde (PFA; TAAB Laboratories
1020 Equipment, Aldermaston, UK). The brainstems were excised and post-fixed with 4% PFA in PBS
1021 overnight at 4°C. The tissues were cryoprotected by soaking in 20% sucrose/PBS for 24 hours and
1022 in 30% sucrose/PBS for additional 24 hours at 4°C. Fixed brainstems were frozen in optimal cutting
1023 temperature (OCT) compound (Sakura Finetek, Tokyo, Japan) and cut into 16 μm-thick coronal
1024 sections using a cryostat (CM3050S; Leica Microsystems, Wetzlar, Germany). Sliced sections were
1025 permeabilized and blocked with 0.1% Tween-20 and 4% donkey serum (Merck Millipore,

1026 Burlington, MA) in Tris-buffered saline, blocked with, and stained by incubating with primary
1027 antibodies at appropriate dilutions followed by their species-matched secondary antibodies. Cell
1028 nuclei were stained with DAPI (Sigma-Aldrich). The slides were mounted with ProLong Gold
1029 Antifade Reagent (Thermo Fisher Scientific) and images were captured with a BZ-9000 digital
1030 microscope system (Keyence, Osaka, Japan).

1031 For immunocytochemistry, cultured cells were fixed with 4% PFA in PBS for 20 minutes at
1032 room temperature (RT) and permeabilized and blocked with 0.1% Triton X-100 and 10% FBS
1033 (Thermo Fisher Scientific) in PBS for 30 minutes at RT. The cells were then incubated with primary
1034 antibodies for 2 hours and then with secondary antibodies for 1 hour at RT.

1035

1036 **Quantitative PCR Analysis (reverse transcription and real-time PCR).** 500 ng of total RNA
1037 extracted from cell culture were subjected to reverse transcription, using ISOGEN II (NIPPON
1038 GENE, Tokyo, Japan) and PrimeScript RT reagent Kit (TaKaRa, Kusatsu, Japan). The resulting
1039 cDNA was subjected to real-time PCR analysis using glyceraldehyde-3-phosphate dehydrogenase
1040 (GAPDH) as an internal control in Applied Biosystems 7500 Real Time PCR System with Power
1041 SYBR Green PCR Master Mix (Thermo Fisher Scientific).
1042 The primers (sense and antisense, respectively) were as follows: mouse *Agtr1a* (AT1R-encoding
1043 gene); 5'-AAAGGCCAAGTCGCACTCAAG-3'

1044 and 5'-TCCACCTCAGAACAAGACGCA-3',

1045 mouse *Gapdh* (GAPDH-encoding gene); 5'-GCAAAGTGGAGATTGTTGCCAT-3' and

1046 5'-CCTTGACTGTGCCGTTGAATTT-3', WPRE (for genomic titration of purified AAV9 vectors);

1047 5'-CTGTTGGGCACTGACAATTC-3' and 5'-GAAGGGACGTAGCAGAAGGA-3'.

1048

1049 **Fluorescent Ang II binding assay.** Six or twenty-four hours after the termination of FSS

1050 application, cultured astrocytes were incubated with Ang II type 2 receptor inhibitor, PD123319

1051 (10^{-6} mol/L in PBS; ab144564, Abcam), for 20 minutes, and then with tetramethylrhodamine

1052 (TAMRA)-labeled Ang II (10^{-8} mol/L in PBS; AS-61181, AnaSpec, Fremont, CA) for 30 minutes.

1053 After 3 times wash with PBS, samples were fixed and subjected to anti-GFP immunostaining to

1054 strengthen the GFP-derived green fluorescence signals and corroborate our analysis on astrocytes

1055 prepared from astrocyte-GFP mice as well as to secure the binding of fluorescent Ang II. Green and

1056 red fluorescence was viewed with a fluorescence microscope (BZ-9000 HS, Keyence). Samples

1057 from astrocytes left unexposed to FSS were prepared and viewed likewise, and provided an

1058 experimental control.

1059

1060 **Hindrance of interstitial fluid movement (flow) by introduction of hydrogel in rat RVLM.** Just

1061 before use, a pre-mixture of polyethylene glycol (PEG) with functional groups (25 g/L in PBS) was

1062 prepared from tetra-armed thiol-terminal (TetraPEG-SH) (Yuka-Sangyo, Tokyo, Japan) and
1063 acrylate-terminal (Tetra-PEG-ACR) (JenKem Technology, TX, USA) PEG solutions as we
1064 previously described[24]. Tetra-armed polyethylene glycol without functional groups (25 g/L in PBS)
1065 was used as an ungelatable control. For the analysis of hydrogel distribution in rat RVLM, we used
1066 Tetra-PEG-SH fluorescently labeled with a thiol-reactive probe (Merck KGaA, Darmstadt,
1067 Germany). Microinjection of PEG solutions into rat RVLM was conducted as described above.
1068 To specifically analyze the consequences of PHM and hydrogel introduction by minimizing
1069 possible invasive influences of microinjection itself, we gave 1-week recovery time before the first
1070 BP measurement, and then applied PHM to the rats (daily 30 minutes, 14 or 28 days). Immediately
1071 subsequent to post-PHM 24-hour urine collection (Fig. 6a), rats were sacrificed by transcardial
1072 infusion of PFA and subjected to histological analysis.
1073
1074 **Terminal deoxynucleotidyl transferase-mediated dUTP nick-end labeling (TUNEL) assay.** Rat
1075 RVLM sections were stained using a TUNEL kit (Biotium, Fremont, CA) according to the
1076 manufacturer's protocols, counterstained with DAPI, and then viewed using a 20x objective with a
1077 fluorescence microscope (BZ-9000 HS, Keyence). The nuclei of apoptotic cells were determined by
1078 the existence of green fluorescent patches, and cell apoptosis was quantified by referring their
1079 counts to total numbers of nuclei defined by DAPI staining.

1080

1081 **Measurement of accelerations at human head.** To measure the accelerations at the human head

1082 during treadmill running or VOCR, we fixed an accelerometer (NinjaScan-Light; Switchscience,

1083 Tokyo, Japan) on foreheads with a surgical tape. Vertical acceleration was evaluated using the

1084 software application provided from the manufacture.

1085

1086 **Blood sampling and measurement of parameters in plasma and serum of humans.** Blood

1087 sampling in the human study of protocol 2 was conducted between 12 PM and 3 PM. Participants

1088 were rested in a sitting position for at least 10 minutes before starting the sampling procedures.

1089 After plasma (for catecolamines and renin activity) and serum (for aldosterone and CRP) separation

1090 by centrifugation, we outsourced the measurement of parameters be tested (BML, Kawagoe, Japan).

1091

1092 **Design and participants of clinical study on antihypertensive effects of vertically oscillating**

1093 **chair riding.** We conducted single-arm clinical studies. The study of protocol 1 (Extended Data

1094 Fig. 5c) was carried out at the affiliated health services facility of Iwai Medical Foundation (Iwai

1095 Keiaien, Tokyo, Japan). The study of protocol 2 (Extended Data Fig. 5d) was carried out at the

1096 National Rehabilitation Center for Persons with Disabilities Hospital.

1097 Subjects were considered eligible if they were 20−75 years old of age and confirmed to have

1098 130−160 mm Hg of SBP at the time of interview for informed consent and eligibility check.
1099 Subjects with mental or psychological illnesses, history or presence of cardiovascular events,
1100 history or presence of severe dysfunction/disorder of liver, kidney, lung, gastrointestinal tract, and
1101 spine, or presence of acute injuries/diseases (e.g., recent traumas and infectious diseases) were
1102 excluded with the exception of those who were given permission for participating in this study from
1103 their primary care physicians. Whereas antihypertensive medication did not disqualify the subjects
1104 (Supplementary Table 2), they were advised not to change their medication from at least one month
1105 prior to the first bout of VOCR through the study period (i.e., up to 8 weeks after the last bout of
1106 VOCR). At a certain (approximately fixed) time point in the morning (typically just before
1107 breakfast), they conducted 3 consecutive measurements of BP (mm Hg) and HR (bpm) using an
1108 automated upper arm-cuff sphygmomanometer, and recorded the values from all those
1109 measurements. These procedures of BP measurement and recording accord with the Japanese
1110 Society of Hypertension Guidelines for the management of hypertension (JSH2019)[72]. Subjects
1111 were directed to start periodical (≥3 days per week) BP/HR measurements at least 2 weeks before
1112 the initiation of the intervention (i.e., daily VOCR) and continue to measure BP/HR throughout the
1113 study period using the same sphygmomanometers. Particularly at the study of protocol 2 (i.e., the
1114 study at the National Rehabilitation Center for Persons with Disabilities), participants were advised
1115 to record all the data of those measurements. Those whose BP lowered below the eligibility

1116 requirement of the study (≥130 mm Hg of SBP) prior to the initiation of VOCR intervention were
1117 eliminated from the study. Participants were directed to be rested and keep calm for at least 1
1118 minute before starting to measure BP/HR. The mean BP/HR value from 3-time measurements was
1119 defined as "value of the day", and used for statistical analysis. When BP and HR were measured
1120 and recorded on ≥3 days during a particular week in the study of protocol 2, the mean of all the
1121 "value of the day"s through the week was defined as "value of the week". For the participants who
1122 agreed. periodical BP/HR measurement and recording (≥3 days per week) was extended up to 8
1123 weeks after the last bout of VOCR.
1124
1125 **Statistical analysis.** All the quantitative data are presented as mean ± s.e.m. Parametric statistical
1126 analyses were conducted by paired or unpaired two-tailed Student's *t*-test for two-group
1127 comparison, and ANOVA with Tukey's post hoc test for multiple (≥3) group comparison, using
1128 Prism software (Version 8, GraphPad Software, San Diego, CA). Differences were considered as
1129 significant at *P* values below 0.05.